THE ASTROPHYSICAL JOURNAL, 404:643–662, 1993 February 20

MOLECULAR CLOUD CORES IN THE ORION A CLOUD. I. NOBEYAMA CS (1–0) SURVEY

KEN'ICHI TATEMATSU,[1,2] TOMOFUMI UMEMOTO,[1] OSAMU KAMEYA,[1,3] NAOMI HIRANO,[1,4] TETSUO HASEGAWA,[5] MASAHIKO HAYASHI,[6] TAKAHIRO IWATA,[7] NORIO KAIFU,[8] HITOMI MIKAMI,[9] YASUHIRO MURATA,[1,10] MAKOTO NAKANO,[11] TAKENORI NAKANO,[1] NAGAYOSHI OHASHI,[1,9] KAZUYOSHI SUNADA,[1,6] HIROSHI TAKABA,[7] AND SATOSHI YAMAMOTO[9]

Received 1992 May 21; accepted 1992 August 31

ABSTRACT

A first high-resolution survey of molecular cloud cores in the Orion A giant molecular cloud is reported. We identified 125 molecular cloud cores from an analysis of the spatial and velocity distribution of the CS (1–0) emission. The cores are generally elongated along the filamentary molecular cloud, and the axial ratio is about 0.5. The mass spectrum index of the cores is -1.6 for $M \geq 50\ M_\odot$. The physical properties of the cores identified in Orion are compared with those of cores in dark clouds reported in the literature. The average radius of the cores in the Orion A cloud, 0.16 pc, is comparable to that of the cores in dark clouds. In contrast, the Orion A cloud contains molecular cloud cores with large line widths (1–2 km s^{-1} FWHM) and large masses ($M > 100\ M_\odot$), which are rarely observed in dark clouds. We suggest that the line width–radius relation differs between these two samples. Within the Orion A cloud the CS line width, core mass, average density, and core-to-core velocity dispersion all decrease toward the south. These trends can be seen, even when the cores with young stellar objects are excluded from the sample. We discuss the implications of the line width–radius relation, and suggest that cores in giant molecular clouds are bounded by higher external pressure, which eventually leads to massive star formation.

Subject headings: ISM: clouds — ISM: individual (Orion Nebula) — ISM: molecules — radio lines: molecular: interstellar — stars: formation

1. INTRODUCTION

It has been pointed out that only low-mass stars are born in dark clouds (cloud mass $\sim 10^3\ M_\odot$), whereas giant molecular clouds (cloud mass $\sim 10^5\ M_\odot$) have a potential of forming massive stars (e.g., Cohen & Kuhi 1979; Larson 1982). It appears that this difference in stellar mass depends on the nature of the molecular cloud where stars are born. In the last decade, observational studies of dark clouds have clearly shown that ~ 0.1 pc–sized, high-density ($n \sim 10^4$–10^5 cm^{-3}) molecular cloud cores (dense cores) are sites of star formation (e.g., Myers, Linke, & Benson 1983; Myers & Benson 1983; Beichman et al. 1986; Myers et al. 1988). It would be fruitful to compare the physical properties of molecular cloud cores in giant molecular clouds with those in dark clouds. However, the observational studies of cores in giant molecular clouds have been extremely limited. Myers and his collaborators used the Palomar Sky Survey photographs to select candidates for molecular cloud cores in dark clouds (e.g., Myers et al. 1983). However, such technique cannot be used for giant molecular clouds because they are much more opaque and more distant. Extensive, unbiased observations are therefore essential to search for high-density molecular cloud cores in giant molecular clouds.

The Orion A cloud, the nearest giant molecular cloud (450 pc; e.g., Genzel & Stutzki 1989), is one of the best targets for a survey of molecular cloud cores. Even for this famous molecular cloud, previous high–angular-resolution studies are limited to the region near Orion KL (e.g., Batrla et al. 1983; Hasegawa 1987). Because the Orion A cloud is 3 times as distant as nearby dark clouds such as the Taurus-Auriga and Ophiuchus regions, a large millimeter-wave telescope is highly desirable to resolve molecular cloud cores. Lada, Bally, & Stark (1991) surveyed molecular cloud cores in the Orion B cloud (L1630), adjacent to the Orion A cloud, in CS (2–1), but only half of the detected cores were resolved with their beam size ($\sim 1'.8$, or 0.21 pc).

Observations of molecular cloud cores biased to young stellar objects (YSOs) are not suitable for our purpose, because cores associated with YSOs might have largely lost their original properties. The line widths of cores with YSOs are known to be broader than those of cores without YSOs, probably owing to interaction with stellar winds/outflows from YSOs (Beichman et al. 1986; Myers et al. 1988; Zhou et al. 1989).

In this paper we report the first systematic survey of molecular cloud cores in the Orion A giant molecular cloud with the 45 m telescope of the Nobeyama Radio Observatory. We observed the CS (1–0) line within 2500 $arcmin^2$ regions with high spatial resolution (36″ beam and 40″ grid spacing) to search for molecular cloud cores. The beam size for the CS (1–0) line corresponds to a linear size of 0.08 pc, which is smaller than the typical size of dark cloud cores. From the data

[1] Nobeyama Radio Observatory, Nobeyama, Minamisaku, Nagano 384-13, Japan.
[2] Present address: Department of Astronomy, University of Texas at Austin, Austin, TX 78712.
[3] National Astronomical Observatory, Mizusawa, Iwate 023, Japan.
[4] Laboratory of Astronomy and Geophysics, Hitotsubashi University, Kunitachi, Tokyo 186, Japan.
[5] Institute of Astronomy, University of Tokyo, Mitaka, Tokyo 181, Japan.
[6] Department of Astronomy, University of Tokyo, Bunkyo-ku, Tokyo 113, Japan.
[7] Kashima Space Research Center, Communications Research Laboratory, Kashima, Ibaraki 314, Japan.
[8] National Astronomical Observatory, Mitaka, Tokyo 181, Japan.
[9] Department of Astrophysics, Nagoya University, Chikusa-ku, Nagoya 464-01, Japan.
[10] Present address: Institute of Space and Astronautical Science, Yoshinodai, Sagamihara, Kanagawa 229, Japan.
[11] Department of Earth Science, Faculty of Education, Oita University, Oita 870-11, Japan.

we derive core properties accurately and compare them with core properties in dark clouds. Observations in ^{13}CO (1–0) were carried out simultaneously to obtain the distribution of less dense molecular gas where molecular cloud cores are embedded. Because the mass of stars being born seems to vary from place to place within the Orion A cloud, we also compare the properties of cores for different regions in the cloud. We derive the mass spectrum of molecular cloud cores in Orion, and discuss its implications. Finally, we discuss a possible relationship between the core properties and the resulting stellar mass. Detailed discussion on the properties of young stellar objects associated with the molecular cloud cores will be presented in a separate paper (Umemoto et al. 1993).

2. OBSERVATIONS

Mapping observations were carried out with the 45 m radio telescope of the Nobeyama Radio Observatory[12] between 1990 May and 1991 June. The $J = 1$–0 transitions of CS (49 GHz) and ^{13}CO (110 GHz) were simultaneously observed. The half-power beamwidth (HPBW) of the telescope was 36″ at 49 GHz and 15″ at 110 GHz. The main-beam efficiencies at 49 and 110 GHz were 0.60 and 0.38, respectively. We used a 7 mm SIS receiver (Tsuboi 1991) for CS (1–0). For ^{13}CO we mainly used a 3 mm Schottky receiver, but occasionally employed a 3 mm SIS receiver. The single-sideband system temperature was typically 500–650 K for CS and 600–1000 K for ^{13}CO. We used the acousto-optical spectrometers with 37 kHz resolution. The grid spacing of the map was 40″ (0.087 pc at a distance of 450 pc), and a total of 5657 positions were observed. The area of the observations was selected to cover a large portion of the ridge of the Orion A cloud on the basis of the ^{13}CO map by Bally et al. (1987). The rms noise level at 0.3 km s^{-1} resolution was 0.34 ± 0.05 K for CS and 0.29 ± 0.10 K for ^{13}CO (average $\pm$ 1 σ deviation).

Additional CS (2–1) and C^{18}O (1–0) observations were carried out toward 21 and 14 positions, respectively. The receivers employed were the 3 mm SIS receiver (1990 December) and the 3 mm Schottky receiver (1991 April). At 98 GHz (CS 2–1), the half-power beamwidth of the telescope was 18″ and the main-beam efficiency was 0.46. Positions for these observations were selected from the local CS (1–0) maxima (peaks of molecular cloud cores) observed in 1990. Because the mapping observations started from the northern end of the Orion A cloud, cores observed in CS (2–1) and C^{18}O are mostly located in the northern portion of the mapped regions.

All spectra were obtained in the position-switching mode. In mapping observations we observed an emission-free position 3 times during a set of 11 on-source observations, and shared emission-free spectra for these 11 on-source spectra. Linear baselines were subtracted from all the spectra. The telescope pointing was measured to be accurate to 5″ by observations of Orion KL (SiO maser) in 43 GHz SiO $J = 1$–0 every 1.5 hr. The line intensity is expressed in terms of T_A^* (Ulich & Haas 1976), which is the antenna temperature corrected by the standard chopper-wheel method. We observed a map center, Orion KL (R.A. [1950] = $5^h32^m47^s$, decl. [1950] = $-5°24'23''$), at least once every day to compensate for the daily variation in the intensity scale. The intensity in Orion KL was 10.0 K T_A^* for CS (1–0) and 11.8 K T_A^* for ^{13}CO.

[12] The Nobeyama Radio Observatory is a branch of the National Astronomical Observatory, an interuniversity research institute operated by the Ministry of Education, Science, and Culture, Japan.

3. GAS DISTRIBUTION

Figure 1 shows a CS (1–0) map of the peak antenna temperature. The surveyed areas are bordered by thin straight lines. As is well known (Maddalena et al. 1986; Bally et al. 1987), the Orion A giant molecular cloud shows a remarkable filamentary structure elongated in the northwest-southeast direction, which is roughly parallel to the Galactic plane. The northern intense part (decl. $-4°50'$ to $-6°20'$) of the cloud is known as the "∫-shaped filament" (e.g., Bally et al. 1987). The Orion Nebula overlaps the ∫-shaped filament from decl. $-5°10'$ to $-5°40'$. The brightest line emission for both ^{13}CO and CS (1–0) is observed in this region.

3.1. *Distribution of Lower Density Gas*

Figure 2 compares a peak ^{13}CO map with the peak CS (1–0) map for the ∫-shaped filament. Because the ^{13}CO emission largely fills the observed areas, lower level contours are omitted from the ^{13}CO map. Although the ^{13}CO emission is rather smoothly distributed, we still observe clumpy structures with a size of ~8′ (1 pc) along the molecular ridge. Dutrey et al. (1991) previously reported a periodic density structure along the ∫-shaped filament on the basis of their integrated C^{18}O (1–0) map, and the structure we observed in ^{13}CO is basically the same as that found by them. The ^{13}CO clumps listed by Bally et al. (1987) are likely to belong to the same class. Here we call such ~1 pc–sized structures *clumps*. On Figure 2 four clumps are recognized, whose centers are roughly placed with the same interval at (R.A., decl.) = ($5^h32^m40^s$, $-5°38'$), ($5^h32^m30^s$, $-5°47'$), ($5^h32^m45^s$, $-6°0'$), and ($5^h33^m10^s$, $-6°7'$). The first and second are not very striking solely on the present peak ^{13}CO map, but previous ^{13}CO column density maps (Schloerb & Loren 1982, 2.3 resolution; Castets et al. 1990, 1.7 resolution), the C^{18}O map of Dutrey et al. (1991, 1.7 resolution), and our peak CS map consistently show that these are separate features. Using the integrated ^{13}CO intensity of our data, we measured the typical size of the clumps across the filament to be about 0.7 pc (5′) FWHM. The average interval of the clump centers is about 1.4 pc (11′). The size of the clumps along the filament is not easy to derive, because the peak ^{13}CO intensity decreases only by 20%–50% around valleys between clumps. Here we take the clump interval, 1.4 pc, as the extent of the clumps along the filament. The ^{13}CO integrated intensity toward the clump centers is 22 ± 4 K km s^{-1} (average $\pm$ 1 σ deviation). Following the method of Bally et al. (1987) and assuming an excitation temperature of 30 K, we obtain $N(H_2)$ $\sim(5 \pm 1) \times 10^{22}$ cm^{-2} and the mass of each clump to be $1000 \pm 200\ M_\odot$.

Dutrey et al. (1991) estimated the typical size of structure to be 7′ × 4′ (0.9 pc × 0.5 pc) and the spacing to be 7′–9′ (0.9–1.2 pc). Our estimates of the extent and interval (1.4 pc × 0.7 pc extent and 1.4 pc interval) are somewhat larger than thoss of Dutrey et al. (1991). The former is possibly due to larger optical depth of ^{13}CO.

One may think that this chain of clumps has been formed by gravitational instability of a filamentary cloud. The observed ^{13}CO line width (FWHM), 2.6 ± 0.2 km s^{-1}, and the line density of order 700 $M_\odot$ pc^{-1} indicate that the filamentary cloud is close to equilibrium. It is known that an equilibrium filamentary cloud is gravitationally unstable for wavelengths larger than the critical value of about twice its diameter (e.g., Larson 1985). The fragmentation is marked when the wavelength is about 5 times the diameter (Bastien 1983). The

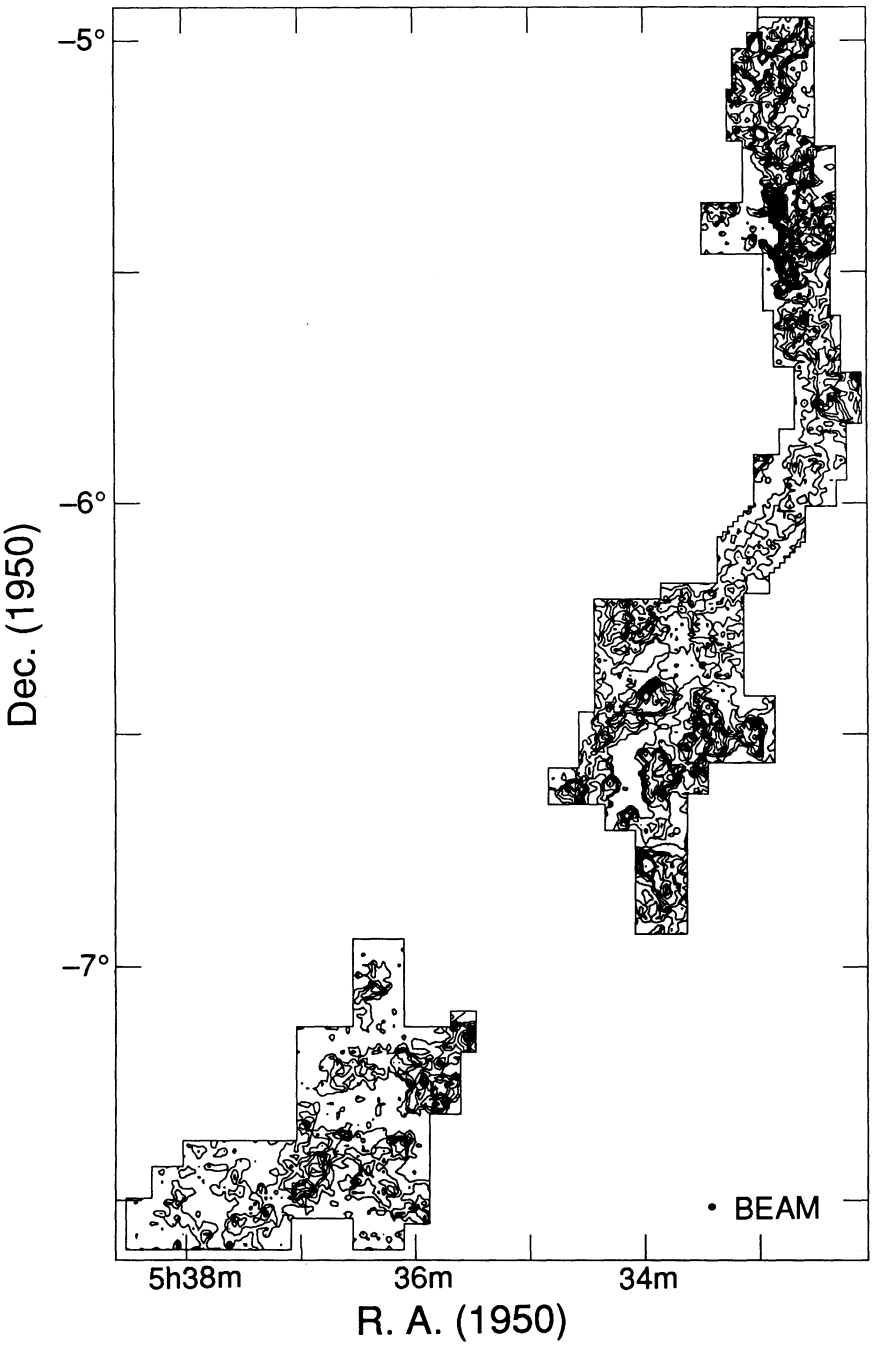

FIG. 1.—A CS (1–0) map of the peak intensity (T_A^*) in V_{LSR} = 2.5–13.5 km s^{-1} in the Orion A cloud. Contour levels are 0.34 K (1 σ) × (3, 4, 5, 6, 7, 8, 9, 12, 15, 18, ..., 33). Thin straight lines delineate the boundary of the surveyed areas. The spectra were convolved to 0.3 km s^{-1} resolution before measuring the peak intensity.

observed ^{13}CO line width and an estimated average surface density of order 10^3 $M_\odot$ pc^{-2} give a critical mass for gravitational instability of $\sim$800 $M_\odot$ according to the formula compiled by Larson (1985). The typical mass of the four clumps above is estimated to be 10^3 $M_\odot$, which is nearly equal to the critical mass. The observed interval of the clumps is about twice as small as the wavelength of the most unstable model for gravitational instability. This factor of 2 difference in wavelength might be explained when we take into account the angle between the line of sight and the filament (e.g., Genzel & Stutzki 1989), the effects of rotation and magnetic fields on the stability of the filament (e.g., Larson 1985; a comparison of numerical results and the ∫-shaped filament is given in Hanawa et al. 1993), and the uncertainty in the estimates of physical parameters.

The Orion A cloud has systematic velocity structures. A velocity gradient (0.135 km s^{-1} pc^{-1}) is observed along the filament (e.g., Kutner et al. 1977). Furthermore, a velocity gradient also can be seen across the filament. In order to eliminate the systematic velocity gradient *along* the filament, we calcu-

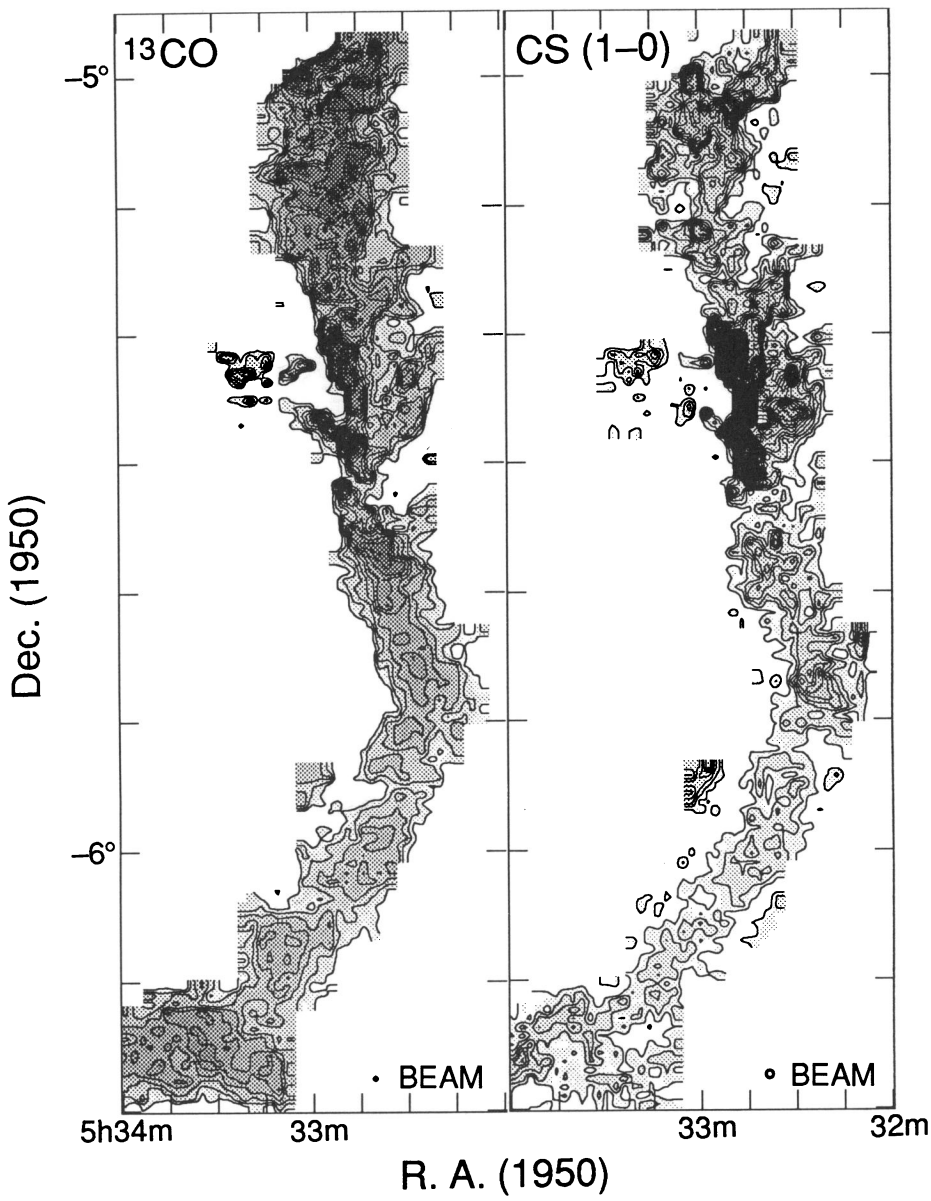

FIG. 2.—Maps of the peak ^{13}CO (1–0) and CS (1–0) intensities (T_A^*) in V_{LSR} = 2.5–13.5 km s^{-1} for the ∫-shaped filament in the Orion A cloud. For ^{13}CO the lowest level is 4.0 K (14 σ), and the level interval is 0.8 K (3 σ). For CS (1–0) the lowest level is 1.02 K (3 σ), and the level interval is 0.34 K (1 σ). The spectra were convolved to 0.3 km s^{-1} resolution before measuring the peak intensity.

late the mean velocity for each declination by averaging spectra at the same declination. Figure 3 shows a velocity-offset map of ^{13}CO. The thin and thick contours, respectively, illustrate 1–2 km s^{-1} blueshifted and redshifted gas with respect to the mean radial velocity at the same declination. We find patterns which suggest the existence of a systematic velocity gradient across the filament. At $-6°05' <$ decl. $< -5°45'$, the thick contours (redshifted) are clearly located on the western side of the thin contours (blueshifted). The velocity gradient has the same sense as that in the southernmost part of the Orion A cloud (decl. $\lesssim -7°$) pointed out by Uchida et al. (1991). On the other hand, at decl. $> -5°20'$ the thick contours (redshifted) seem to be located on the eastern side of the thin contours (blueshifted), in contrast with the above. One may interpret the change in the sense of the velocity gradient in terms of the twisting motion of the filaments. The velocity gradient is estimated to be ~2–4 km s^{-1} pc^{-1} from ^{13}CO position-velocity diagrams (not shown). The relative velocity at the filament periphery (~0.5 pc from the axis) is of order 1–2 km s^{-1}: this is close to the value of 2.3 km s^{-1} which is necessary to support the cloud against gravity if it means rotation. It is possible that this rotation as well as turbulent gas motion plays an important role in supporting the filamentary cloud against the self-gravity.

3.2. *Distribution of High-Density Gas*

We selected the 49 GHz CS (1–0) line to obtain the distribution of high-density (10^4–10^5 cm^{-3}) gas. It is known that CS is a rather robust molecule for interstellar chemical processes (Herbst & Leung 1989) and is widely detected toward high-density gas condensations. Furthermore, the line intensity from CS is moderately intense. Compared with lines of higher

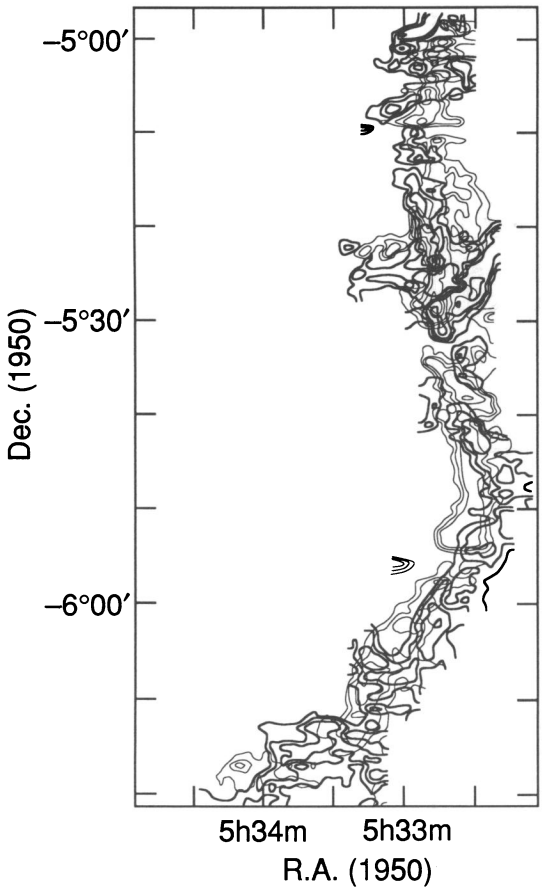

FIG. 3.—Velocity-offset ^{13}CO map of the ∫-shaped filament. The thin contours represent a map of $\Delta V_{LSR} = -2$ to -1 km s^{-1}, and the thick contours represent a map of $\Delta V_{LSR} = 1$–2 km s^{-1}. The contour levels are 2, 3, 4, 6, and 8 K km s^{-1}.

rotational levels, CS (1–0) has an advantage of detecting cores without YSOs because such cores are not highly excited. The line also has a lower optical depth (Linke & Goldsmith 1980; Snell, Langer, & Frerking 1982), which is helpful in estimating physical parameters. These advantages make CS (1–0) one of the best molecular lines for surveys of molecular cloud cores.

Figure 1 shows that there are many local condensations in the Orion A cloud. The typical size (FWHM diameter) of these condensations is roughly 1′–4′ (0.1–0.5 pc). We catalog well-defined molecular cloud cores from these condensations (§ 4.1).

To know how the intensity distribution depends on the employed molecular line, we compare the CS distribution with that of NH_3, which is also used to investigate the distribution of high-density gas (e.g., Benson & Myers 1989). Figure 4 compares a part of our CS (1–0) map for the region near Orion KL with the NH_3 (1, 1) map of Batrla et al. (1983). The telescope beam employed by them (43″) is comparable to ours (36″), but the area of the NH_3 observation is limited to the vicinity of the Orion Nebula. Both maps show local condensations with a size (diameter) of 1′–2′, or 0.1–0.3 pc. Positions of local intensity peaks in these two lines generally coincide with each other, but the intensity ratio of CS (1–0) to NH_3 (1, 1) varies drastically from core to core. Roughly speaking, NH_3 is more intense to the north of Orion KL, while CS is stronger to the south of KL. In particular, an intense CS core (R.A. $5^h32^m47^s$, decl. −5°28′20″) located ∼2′ south of S6 is not seen in NH_3 (1, 1) although this core is located within the area observed by Batrla et al. Core S6 is much weaker in intensity than Orion KL in NH_3 (1, 1), but is as intense as KL in NH_3 (2, 2) (Batrla et al. 1983); this is probably due to excitation by the newly born star, Orion-S (Ziurys, Wilson, & Mauersberger 1990; Schmidt-Burgk et al. 1990).

Difference in spatial distribution between CS and NH_3 has also been reported for dark cloud cores (Zhou et al. 1989). As a possible origin of such difference, we first consider different excitation conditions for these two molecules. The critical density for the NH_3 (1, 1) line is 10^4 cm^{-3}, which is an order of magnitude lower than that for the CS (1–0) line (10^5 cm^{-3}). Therefore, the NH_3 line should be observed in less dense regions than the CS line. However, NH_3 distribution is not

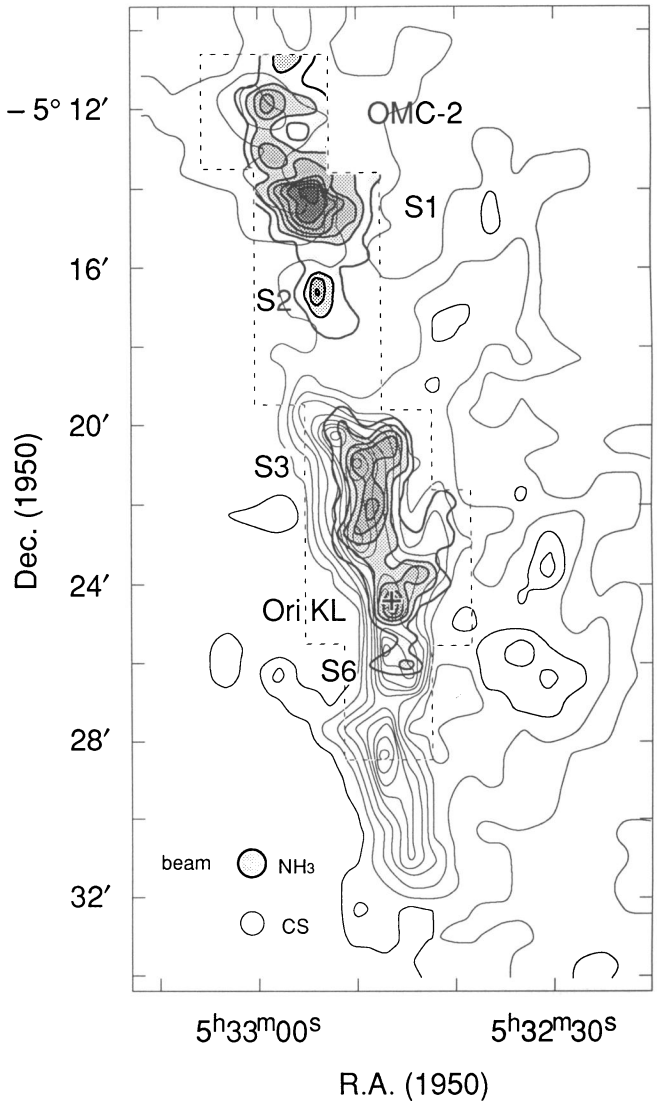

FIG. 4.—NH_3 (1, 1) map (T_{mb}, *gray scale with thick lines*) of Batrla et al. (1983) superposed on our CS (1–0) map (T_A^*, *thin lines*). The NH_3 map was obtained with a 43″ beam and at half-beamwidth spacing. The velocity resolution for the NH_3 observations is 0.8 km s^{-1}, and the CS spectra were convolved to the same resolution. The lowest level is 2 K for NH_3 and 1 K for CS. The level interval is 1 K for both the maps. S1, S2, S3, and S6 were designated by Batrla et al.

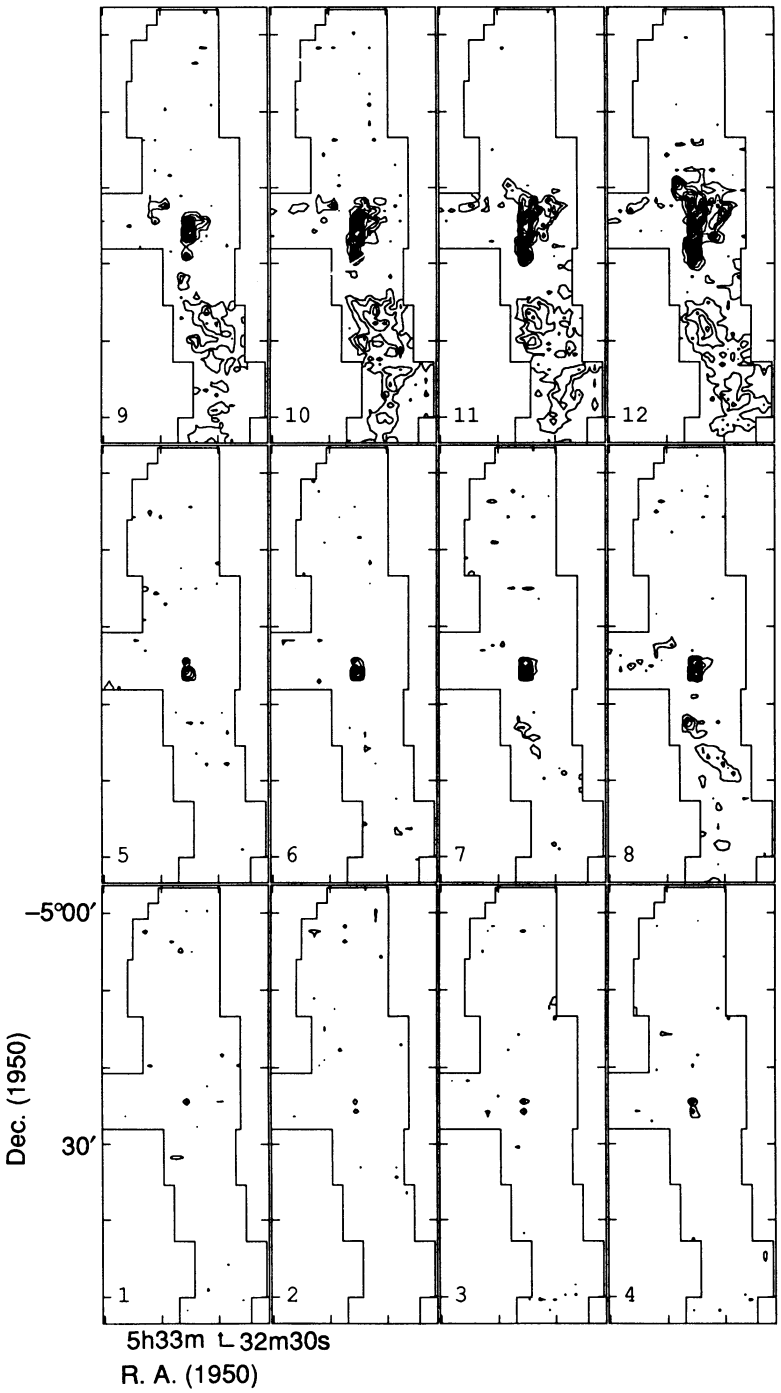

FIG. 5a

FIG. 5.—The 0.5 km s^{-1} interval velocity-channel maps of CS (1–0) shown for three divided regions, regions I, II, and III. The numeral n (ranging from 1 to 22) in the lower left-hand corner of each map represents the V_{LSR} range of integration, $0.5n + 2.0$ to $0.5n + 2.5$ km s^{-1}. The contour interval is 0.39 K km s^{-1} (3 σ). (*a*) Region I, V_{LSR} = 2.5–8.5 km s^{-1}. (*b*) Region I, V_{LSR} = 8.5–13.5 km s^{-1}. (*c*) Region II, V_{LSR} = 5.0–11.0 km s^{-1}. (*d*) Region III, V_{LSR} = 2.5–8.5 km s^{-1}.

always more extended than CS, as shown in Figure 4. Since the CS (1–0) line is not heavily saturated ($\tau < 3$; e.g., Linke & Goldsmith 1980), it seems difficult to explain the compact distribution of NH_3 only in terms of scattered line photons due to a large optical depth of CS (cf. Zhou et al. 1989). Another possibility is chemical abundance variation from core to core (Ungerechts et al. 1992). Such abundance variation among cores has often been pointed out in other regions, such as TMC-1 (Little et al. 1979; Hirahara et al. 1992) and L134N (Swade 1989). On the basis of an extensive survey toward dark cloud cores, Suzuki et al. (1992) pointed out that NH_3 tends to be abundant in star-forming cores. This indicates that the abundance of NH_3 is sensitive to the cloud conditions, and, hence, a survey of cloud cores in NH_3 would naturally be biased to the cores in which stars have already formed. In the present study, we therefore employed the CS line to pick up the

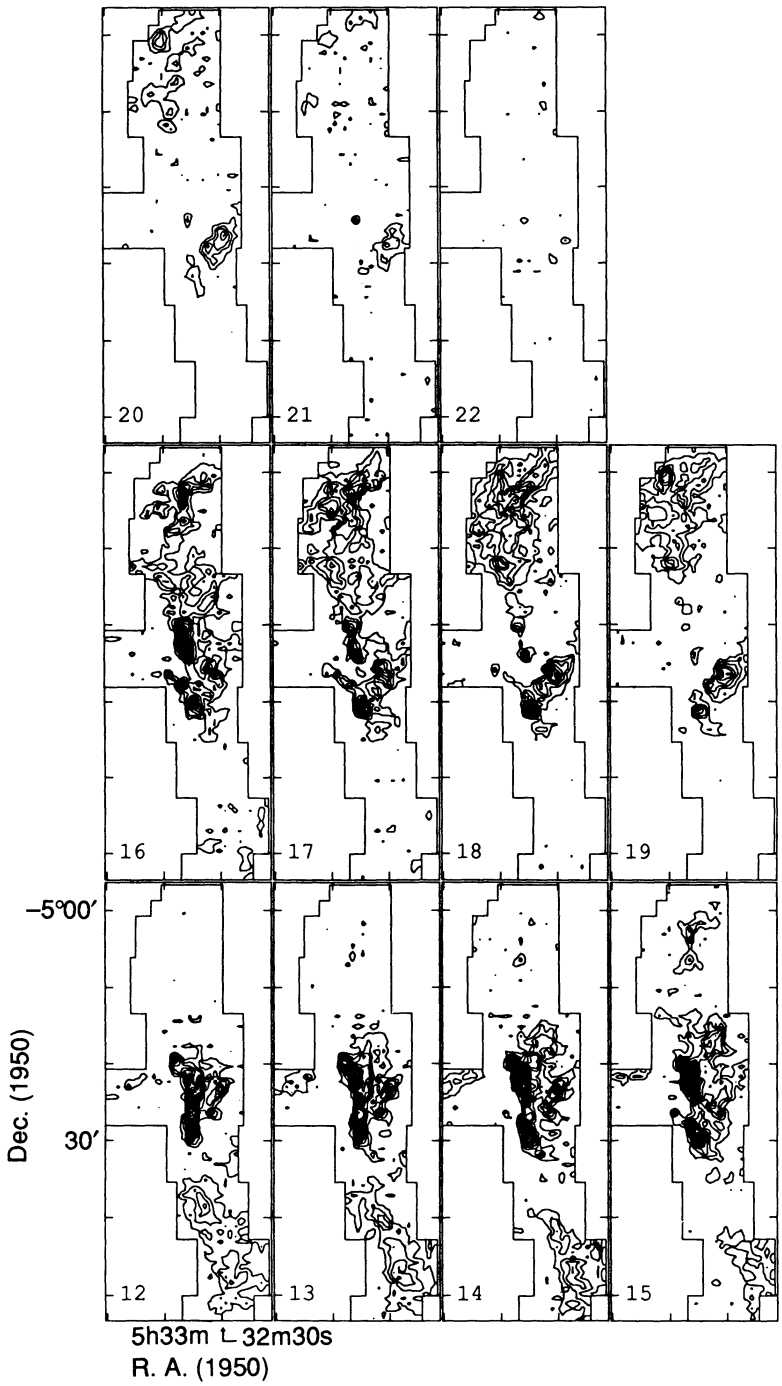

FIG. 5*b*

density maxima in the giant molecular cloud. In order to discuss the origin of the difference in molecular distribution further, it is highly desirable to observe other molecular lines toward the cores identified in the present study.

4. PROPERTIES OF MOLECULAR CLOUD CORES

4.1. *Identification of Cores and Determination of Core Properties*

We identified molecular cloud cores by using the CS (1–0) data with the following procedure.

1. As core candidates we selected local intensity maxima on 0.5 km s^{-1} interval velocity-channel maps. Figure 5 shows channel maps for three divided regions which have similar lengths along the ridge: region I ($-4°55' >$ decl. $\geq -5°50'$), region II ($-5°50' >$ decl. $\geq -6°55'$), and region III ($-6°55' >$ decl. $\geq -7°40'$) (these three regions will be used also to investigate spatial difference in the core properties in the Orion A cloud in § 5.2). We adopted a 5 σ level as the threshold for core candidates. We regarded two maxima as different candidates if the "valley" between them is deeper than 2 σ. Local intensity maxima on map boundary were

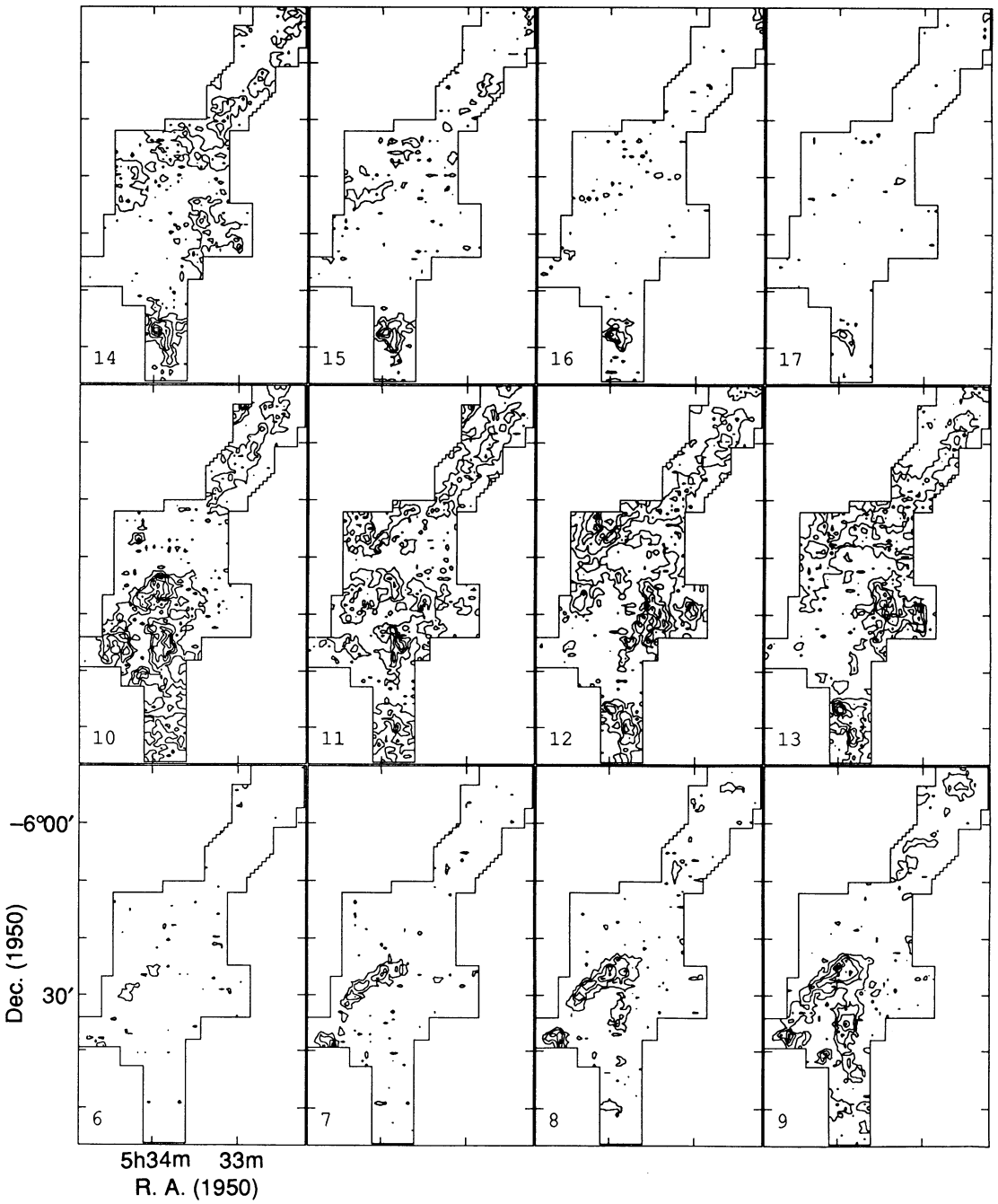

FIG. 5c

excluded because we cannot deduce core properties such as the size.

2. For each candidate, we made four position-velocity (P-V) diagrams passing through the CS (1–0) peak position. For making P-V diagrams, we convolved spectra to 0.3 km s^{-1} resolution to improve the signal-to-noise ratio. Figure 6 shows examples of the P-V diagram.

3. We checked whether a core candidate is separated from others at a 5 σ noise level on each of the four P-V diagrams.

4. In the case in which there are two or more candidates in the 5 σ level contours, we identified them as separate cores if they appear isolated at any of the 10 σ, 15 σ, 20 σ, ... levels on P-V diagrams.

Our procedure aims to search for local high-density condensations, which may lead to star formation in the future or may already have led to star formation. We do not intend to subdivide irregularly shaped cores using a kind of template for the shape of a core (cf. a study of the M17 SW region by Stutzki & Güsten 1990).

A total of 125 molecular cloud cores have been identified. Most of them are newly identified in the present work. Table 1 is the catalog of the molecular cloud cores in the Orion A

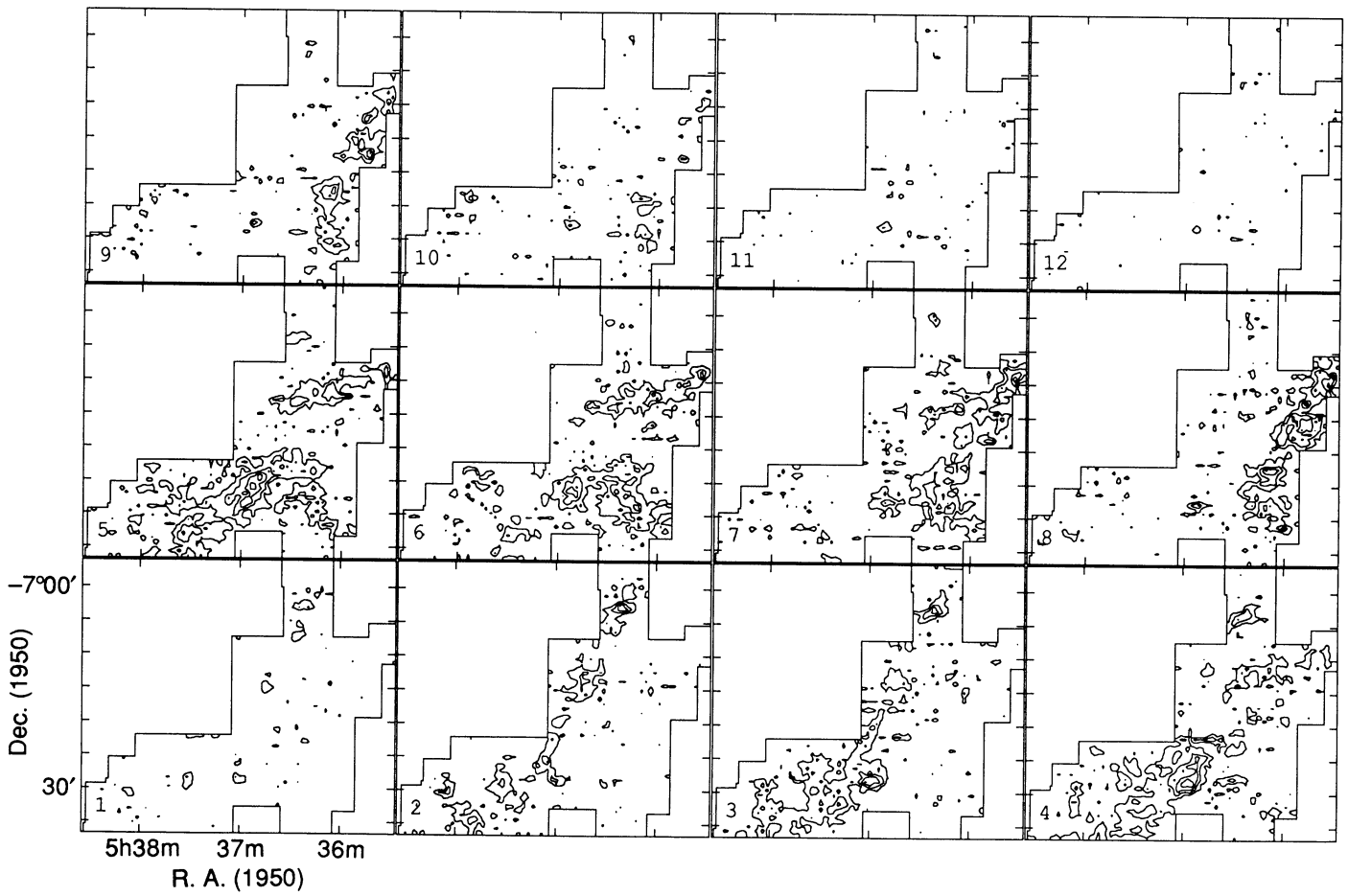

FIG. 5d

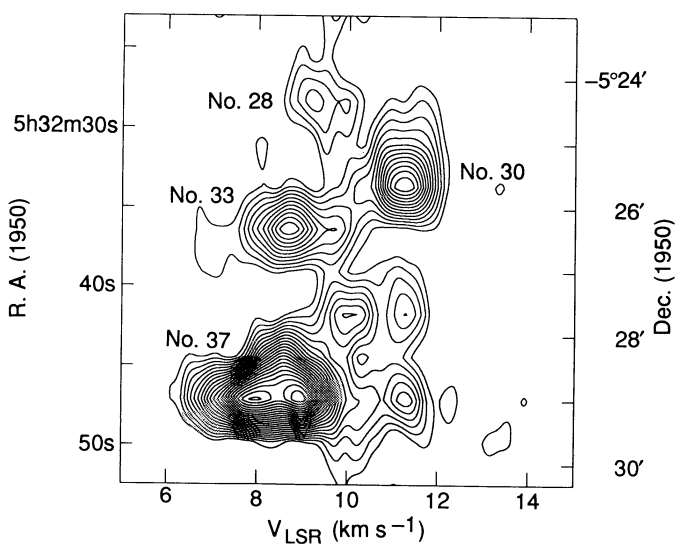

FIG. 6a

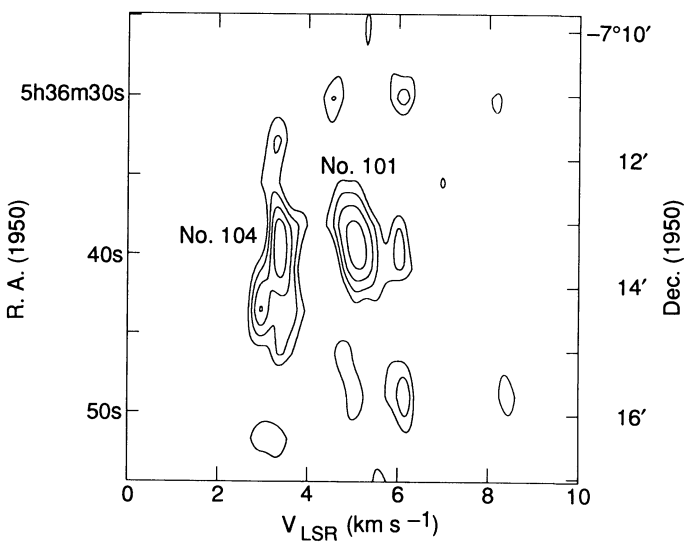

FIG. 6b

FIG. 6.—Two examples of the *P-V* diagram for core candidates. The spectra were convolved to 0.3 km s^{-1} resolution. The lowest contour level and contour interval are 0.68 K (2 σ) and 0.34 K (1 σ), respectively. Each of the strips for the diagrams passes through the peaks of Nos. 30, 33, 101, and 104, but does not pass exactly through the peaks for Nos. 28 and 37.

TABLE 1

CATALOG OF MOLECULAR CLOUD CORES IN ORION A CLOUD

Number	R.A.(1950)	Decl.(1950)	V_{LSR} (km s^{-1})	R (pc)	T_A^*(CS) (K)	Δv(CS) (km s^{-1})	M ($M_\odot$)	M_{vir} ($M_\odot$)	Outflow/*IRAS*
1.....	$5^h32^m52^s.4$	−4°59′03″	11.8	0.15	1.8	1.17	9.3E+1	4.4E+1	05327−0457
2.....	5 33 03.1	−5 01 03	11.7	0.14	4.2	1.01	1.4E+2	2.9E+1	
3.....	5 32 49.7	−5 02 23	10.6	0.23	5.0	1.75	9.1E+2	1.5E+2	
4.....	5 33 00.4	−5 03 03	11.2	0.22	4.0	0.88	2.9E+2	3.5E+1	
5.....	5 33 00.4	−5 05 03	10.8	0.14	4.2	0.82	1.2E+2	2.0E+1	
6.....	5 32 49.7	−5 06 23	10.6	0.20	3.4	2.27	5.8E+2	2.2E+2	
7.....	5 33 11.1	−5 07 43	11.2	0.20	2.9	1.04	1.7E+2	4.4E+1	
8.....	5 32 55.0	−5 09 43	11.3	0.20	2.3	1.93	3.1E+2	1.5E+2	
9.....	5 32 44.4	−5 11 43	10.8	0.17	1.9	1.13	1.1E+2	4.6E+1	
10.....	5 33 11.1	−5 11 43	10.7	0.11	2.3	0.74	1.8E+1	1.2E+1	
11.....	5 32 57.7	−5 12 23	11.2	0.18	3.8	1.33	2.4E+2	6.6E+1	OMC-2
12.....	5 32 36.3	−5 13 03	10.3	0.13	2.2	0.64	2.3E+1	1.1E+1	
13.....	5 33 03.1	−5 13 43	10.3	0.16	2.5	0.76	8.4E+1	2.0E+1	
14.....	5 32 33.6	−5 14 23	10.7	0.14	2.0	1.71	6.9E+1	8.5E+1	
15.....	5 32 49.7	−5 14 23	10.6	0.15	2.0	1.36	8.7E+1	6.0E+1	
16.....	5 32 49.7	−5 16 23	10.0	0.11	2.3	1.68	7.9E+1	6.7E+1	
17.....	5 32 39.0	−5 17 03	9.7	0.26	3.4	1.28	4.7E+2	9.1E+1	
18.....	5 32 49.7	−5 17 43	10.7	0.16	2.2	1.26	9.0E+1	5.2E+1	
19.....	5 32 41.6	−5 19 43	9.2	0.14	4.4	0.84	9.2E+1	2.1E+1	
20.....	5 32 36.3	−5 21 03	10.0	0.11	2.3	1.08	2.7E+1	2.6E+1	
21.....	5 32 49.7	−5 21 03	9.4	0.11	12.2	1.60	5.3E+2	6.0E+1	
22.....	5 32 33.6	−5 21 43	7.9	0.12	2.5	1.14	4.9E+1	3.3E+1	
23.....	5 33 13.8	−5 21 43	9.0	0.12	2.1	1.22	4.5E+1	3.9E+1	
24.....	5 33 27.2	−5 21 43	9.8	0.10	1.9	0.86	1.9E+1	1.5E+1	
25.....	5 32 57.7	−5 22 23	6.9	0.09	2.2	1.82	2.2E+1	6.1E+1	
26.....	5 32 49.7	−5 23 03	9.8	0.11	11.1	1.29	3.6E+2	3.9E+1	
27.....	5 33 19.1	−5 23 03	8.5	0.08	2.1	0.94	1.9E+1	1.4E+1	
28.....	5 32 30.9	−5 23 43	8.8	0.14	5.0	1.65	2.6E+2	7.8E+1	
29.....	5 32 47.0	−5 24 23	8.5	0.15	10.0	3.71	1.8E+3	4.4E+2	Orion KL
30.....	5 32 33.6	−5 25 43	11.2	0.17	5.2	1.19	1.8E+2	5.0E+1	
31.....	5 32 47.0	−5 25 43	6.2	0.10	8.4	2.44	3.2E+2	1.2E+2	Orion-S
32.....	5 33 03.1	−5 25 43	11.2	0.08	1.9	0.89	1.1E+1	1.3E+1	
33.....	5 32 36.3	−5 26 23	8.7	0.08	4.3	1.45	5.1E+1	3.4E+1	
34.....	5 32 57.7	−5 26 23	10.2	0.06	2.9	1.71	3.8E+1	3.8E+1	
35.....	5 32 39.0	−5 27 43	11.5	0.12	3.4	1.23	6.1E+1	3.9E+1	
36.....	5 32 49.7	−5 27 43	10.1	0.07	7.1	1.07	7.7E+1	1.6E+1	
37.....	5 32 47.0	−5 28 23	8.7	0.10	10.5	2.12	6.0E+2	9.7E+1	
38.....	5 33 33.6	−5 29 43	12.2	0.13	1.7	1.57	4.4E+1	7.0E+1	
39.....	5 32 44.3	−5 29 43	9.8	0.11	7.5	0.99	1.2E+2	2.2E+1	05327−0529
40.....	5 32 44.3	−5 31 03	11.2	0.10	6.9	1.01	1.1E+2	2.1E+1	
41.....	5 32 39.0	−5 31 43	9.2	0.10	2.6	1.28	2.7E+1	3.4E+1	
42.....	5 32 49.7	−5 32 23	6.3	0.09	3.3	0.66	3.7E+1	8.5E+0	
43.....	5 32 36.3	−5 33 43	10.8	0.16	2.0	1.67	7.5E+1	9.1E+1	
44.....	5 32 36.3	−5 36 23	7.0	0.13	3.2	1.18	1.1E+2	3.8E+1	
45.....	5 32 49.7	−5 37 03	8.4	0.13	1.9	1.04	4.1E+1	2.9E+1	
46.....	5 32 30.9	−5 37 43	7.0	0.23	2.5	1.64	3.5E+2	1.3E+2	
47.....	5 32 39.0	−5 38 23	8.3	0.29	3.2	0.88	3.9E+2	4.7E+1	
48.....	5 32 41.6	−5 39 43	7.5	0.18	2.4	2.34	2.2E+2	2.0E+2	
49.....	5 32 22.9	−5 41 03	7.5	0.14	2.2	1.64	7.5E+1	7.9E+1	
50.....	5 32 09.5	−5 43 43	9.2	0.14	2.7	0.98	4.1E+1	2.8E+1	
51.....	5 32 28.2	−5 45 03	7.6	0.27	1.9	1.19	2.4E+2	8.1E+1	
52.....	5 32 25.6	−5 47 43	9.0	0.22	3.5	0.76	1.5E+2	2.7E+1	
53.....	5 32 33.6	−5 50 23	7.4	0.21	2.3	0.57	6.9E+1	1.4E+1	
54.....	5 32 41.6	−5 55 03	7.7	0.15	2.0	0.62	1.9E+1	1.2E+1	
55.....	5 32 30.9	−5 55 43	7.9	0.19	2.0	1.29	1.0E+2	6.7E+1	
56.....	5 32 44.3	−5 57 43	7.5	0.15	2.0	1.24	5.5E+1	4.8E+1	
57.....	5 32 36.3	−5 59 43	8.4	0.27	2.1	1.41	2.5E+2	1.1E+2	
58.....	5 32 44.3	−6 01 43	8.2	0.24	2.1	1.14	1.6E+2	6.5E+1	
59.....	5 33 13.8	−6 09 43	8.4	0.33	1.8	1.61	3.8E+2	1.8E+2	05334−0611
60.....	5 33 13.8	−6 11 03	9.0	0.24	1.7	1.34	1.5E+2	9.0E+1	
61.....	5 33 40.6	−6 12 23	8.7	0.20	2.4	1.21	1.5E+2	6.0E+1	
62.....	5 33 37.9	−6 14 23	9.1	0.30	1.9	1.34	3.1E+2	1.1E+2	
63.....	5 34 10.2	−6 15 03	8.2	0.27	2.9	1.32	3.6E+2	9.8E+1	
64.....	5 34 02.0	−6 17 03	8.2	0.21	2.9	1.04	1.7E+2	4.8E+1	
65.....	5 34 10.2	−6 17 03	7.6	0.10	3.1	0.85	3.4E+1	1.6E+1	
66.....	5 34 15.5	−6 19 03	8.9	0.30	2.2	1.34	2.8E+2	1.1E+2	
67.....	5 33 54.1	−6 23 43	6.9	0.22	3.0	1.75	3.3E+2	1.4E+2	L1641-North
68.....	5 33 29.9	−5 24 23	9.3	0.13	2.2	0.71	3.3E+1	1.4E+1	
69.....	5 33 59.5	−6 25 03	6.6	0.15	3.6	1.65	1.9E+2	8.5E+1	Morgan 8
70.....	5 34 18.2	−5 26 23	8.2	0.17	2.8	0.91	6.4E+1	3.0E+1	
71.....	5 33 03.1	−6 28 23	8.6	0.15	3.4	1.01	1.2E+2	3.3E+1	05330−0628 (V801 Ori)
72.....	5 33 27.3	−6 28 23	8.8	0.27	3.7	0.96	3.1E+2	5.2E+1	
73.....	5 34 07.5	−6 28 23	7.3	0.17	2.2	1.75	1.2E+2	1.1E+2	
74.....	5 34 15.6	−6 28 23	6.2	0.19	2.5	1.35	1.4E+2	7.4E+1	
75.....	5 34 15.6	−6 29 43	7.8	0.14	1.8	1.24	4.1E+1	4.6E+1	

TABLE 1—*Continued*

Number	R.A.(1950)	Decl.(1950)	V_{LSR} (km s^{-1})	R (pc)	T_A^*(CS) (K)	Δv(CS) (km s^{-1})	M ($M_\odot$)	M_{vir} ($M_\odot$)	Outflow/*IRAS*
76.....	5 33 35.3	−6 30 23	8.4	0.12	2.7	0.75	3.0E+1	1.4E+1	
77.....	5 34 20.9	−6 30 23	6.2	0.18	2.5	1.49	1.4E+2	8.6E+1	
78.....	5 34 23.6	−6 31 03	7.5	0.12	2.1	1.06	3.4E+1	2.9E+1	
79.....	5 33 38.0	−6 31 43	8.4	0.14	2.8	0.63	2.8E+1	1.1E+1	
80.....	5 33 00.4	−6 32 23	9.0	0.11	2.3	1.16	3.7E+1	3.1E+1	
81.....	5 33 59.3	−6 32 23	7.2	0.15	2.3	1.09	5.6E+1	3.7E+1	
82.....	5 33 51.4	−6 33 03	7.5	0.14	3.0	1.35	8.4E+1	5.2E+1	
83.....	5 34 20.9	−6 33 43	7.2	0.20	2.5	0.70	5.9E+1	2.1E+1	
84.....	5 33 32.6	−6 34 23	8.4	0.12	3.4	0.96	5.5E+1	2.3E+1	
85.....	5 33 54.1	−6 35 03	6.8	0.28	3.7	1.14	3.9E+2	7.7E+1	
86.....	5 34 31.7	−6 35 43	7.4	0.18	2.1	0.75	3.4E+1	2.2E+1	
87.....	5 34 18.3	−6 36 23	7.4	0.18	2.9	0.62	5.4E+1	1.5E+1	
88.....	5 34 34.4	−6 37 43	6.5	0.19	2.9	1.37	1.7E+2	7.6E+1	
89.....	5 34 07.5	−6 40 23	6.9	0.16	2.8	0.83	6.2E+1	2.3E+1	Morgan 18
90.....	5 33 51.3	−6 41 43	7.0	0.17	1.7	1.65	6.1E+1	9.5E+1	
91.....	5 33 59.5	−6 47 03	9.0	0.20	4.1	1.43	3.1E+2	8.4E+1	HH 1–2
92.....	5 33 59.3	−6 47 43	10.0	0.15	3.5	1.17	1.2E+2	4.3E+1	
93.....	5 33 48.8	−6 50 23	8.4	0.23	3.2	1.75	3.1E+2	1.5E+2	
94.....	5 34 02.0	−6 53 03	7.6	0.14	1.9	0.86	3.0E+1	2.2E+1	
95.....	5 36 21.3	−7 02 23	3.5	0.16	2.7	1.49	8.5E+1	7.5E+1	L1641-Center
96.....	5 35 39.0	−7 07 43	6.0	0.10	2.6	0.89	1.9E+1	1.7E+1	
97.....	5 35 33.6	−7 09 03	5.7	0.19	3.3	1.44	1.5E+2	8.1E+1	
98.....	5 35 41.7	−7 10 23	5.9	0.15	2.2	1.46	6.0E+1	6.7E+1	05357−0710 (Haro 14a)
99.....	5 36 03.2	−7 11 43	5.3	0.20	2.2	1.33	8.9E+1	7.4E+1	
100.....	5 35 47.1	−7 12 23	6.4	0.10	2.5	1.27	2.3E+1	3.2E+1	
101.....	5 36 38.2	−7 13 03	5.0	0.15	1.8	0.99	2.7E+1	3.0E+1	
102.....	5 36 07.9	−7 13 43	5.7	0.10	2.0	0.72	8.2E+0	1.1E+1	
103.....	5 36 26.6	−7 13 43	4.9	0.20	1.7	2.05	1.0E+2	1.8E+2	05363−0714 (Haro 4-249)
104.....	5 36 40.9	−7 13 43	3.4	0.19	2.0	0.67	2.8E+1	1.8E+1	
105.....	5 35 41.7	−7 15 03	6.0	0.18	2.3	0.93	5.7E+1	3.2E+1	
106.....	5 35 55.2	−7 15 03	6.4	0.15	2.8	0.58	2.9E+1	1.0E+1	
107.....	5 35 44.4	−7 17 03	6.5	0.18	3.2	0.78	7.1E+1	2.3E+1	
108.....	5 35 49.8	−7 18 23	5.9	0.15	2.3	0.87	3.7E+1	2.3E+1	
109.....	5 36 03.3	−7 18 23	6.1	0.19	2.1	0.75	5.2E+1	2.3E+1	
110.....	5 36 57.0	−7 20 23	3.5	0.14	2.7	0.42	1.2E+1	5.2E+0	
111.....	5 36 35.6	−7 21 43	4.3	0.15	2.1	1.06	3.9E+1	3.6E+1	
112.....	5 36 10.6	−7 22 23	6.2	0.19	2.8	1.11	1.0E+2	5.0E+1	
113.....	5 37 04.1	−7 25 43	3.3	0.12	2.2	0.79	1.6E+1	1.6E+1	
114.....	5 36 24.0	−7 26 23	5.4	0.26	2.6	1.03	1.6E+2	5.8E+1	
115.....	5 36 29.3	−7 27 43	4.4	0.10	2.2	0.82	1.4E+1	1.4E+1	
116.....	5 36 10.6	−7 28 23	5.6	0.22	2.1	1.78	1.6E+2	1.5E+2	
117.....	5 36 53.4	−7 28 23	4.3	0.27	3.2	1.38	3.2E+2	1.1E+2	Haro 4-255
118.....	5 38 03.1	−7 29 03	3.9	0.12	1.7	1.47	2.5E+1	5.5E+1	Re 50
119.....	5 38 03.1	−7 30 23	3.5	0.14	1.8	1.19	3.0E+1	4.2E+1	
120.....	5 36 00.7	−7 31 03	6.2	0.15	2.4	0.99	3.4E+1	3.1E+1	
121.....	5 36 06.0	−7 31 43	4.8	0.13	1.9	0.84	1.7E+1	1.9E+1	
122.....	5 37 17.5	−7 31 43	3.9	0.18	2.6	0.83	4.9E+1	2.6E+1	
123.....	5 37 33.6	−7 32 23	4.6	0.23	1.8	1.16	7.8E+1	6.5E+1	L1641-South 3
124.....	5 38 03.1	−7 32 23	3.8	0.14	1.9	0.77	2.2E+1	1.7E+1	
125.....	5 37 49.7	−7 34 23	3.3	0.18	1.9	0.91	3.5E+1	3.2E+1	

cloud. The radius R is measured as half of the arithmetic average of linear extents (FWHM in the peak intensity) on the four P-V diagrams, and then is corrected for broadening due to the telescope beam ($R = [R_{obs}^2 - (\mathrm{HPBW}/2)^2]^{1/2}$). The peak intensity T_A^* and line width (FWHM) Δv in Table 1 are obtained by fitting a Gaussian (or Gaussians if necessary) to the line profile, which is not smoothed. To estimate the core mass M, we calculate the column density by adopting a formula,

$$N(\mathrm{CS}) = (2.61 \times 10^{12}) \int T_R(\mathrm{CS}\ 1\text{–}0) dv / f_1 \ \mathrm{cm}^{-2} .$$

The fractional population of the $J = 1$ level, f_1, is given by $f_1 = 3.53/T_{ex}$. We use approximations which are good for $T_{ex} \gtrsim 10$ K. The radiation temperature T_R is obtained by dividing T_A^* by the beam efficiency. Since CS (1–0) is considered to be partially thermalized, an estimate of the excitation temperature T_{ex} is not straightforward. Here we adopt an approximation that T_{ex} of CS is equal to that of ^{13}CO (1–0) in view of the modest optical depth and thermalization of the ^{13}CO line. The minimum value of T_{ex} is 8.5 K, and we may safely use the formula of column density estimation above. The CS abundance relative to H_2 is assumed to be 10^{-9}, although it shows deviation among regions (e.g., Graedel, Langer, & Frerking 1982; Blake et al. 1987). We obtain the mass M from the column density: $M = 2.76 m_H (2\pi R^2/3) N(H_2)$. The mass of a core derived from the integrated CS (1–0) intensity ranges from 8 to 1800 $M_\odot$. The mass M obtained in this way is comparable to the virial mass M_{vir}: the average of $\log (M_{vir}/M)$ calculated for each core is -0.29 ± 0.29 (1 σ deviation). Here we adopt a formula, $M_{vir}(M_\odot) = 210 R(\mathrm{pc})\ \Delta v(\mathrm{km\ s^{-1}})^2$. Because various kinds of molecular clouds, including molecular cloud cores, are

TABLE 2

CS (2–1) AND $C^{18}O$ DATA

Number	CS (2–1) T_A^* (K)	CS (2–1) Δv (km s^{-1})	$C^{18}O$ (1–0) T_A^* (K)	$C^{18}O$ (1–0) Δv (km s^{-1})
2.....	1.9	1.51	...[a]	...
3.....	3.0	1.09	...	...
5.....	2.6	1.44	2.2	1.15
6.....	2.7	2.25	1.8	2.84
13.....	0.8	2.58	...	...
15.....	1.4	1.36	1.2	1.31
16.....	1.7	1.63	1.4	1.68
18.....	1.7	1.75	1.0	1.82
19.....	3.6	1.58	...	...
21.....	12.3	2.16	2.8	1.94
26.....	12.4	1.14	1.5	1.19
28.....	2.2	2.21	0.9	2.07
29.....	12.3	3.53	1.3	3.01
31.....	7.1	3.76	...	...
33.....	2.6	1.73	...	...
37.....	12.5	1.91	2.5	1.61
40.....	2.4	1.01	1.0	1.03
41.....	1.9	1.72	0.8	1.19
46.....	1.3	1.85	2.1	1.33
48.....	1.0	2.41	2.2	1.40
70.....	0.8	1.26	...	...

[a] In this table three dots mean "not observed."

generally found to be close to virial equilibrium (e.g., Larson 1981; Myers 1983), this agreement supports the assumptions made in the above derivation of the mass. The correlation between M_{vir} and M will be investigated in § 4.3.

Table 2 lists the results of additional CS (2–1) and $C^{18}O$ observations toward 21 cores. The average physical parameters of the 125 molecular cloud cores are summarized in Table 3.

One might suspect that physical parameters based on the CS (1–0) data might be affected by the optical thickness of the CS (1–0) line. The optical depth of the CS (1–0) line in various kinds of objects is thought not to be heavily saturated ($\tau < 3$; e.g., Linke & Goldsmith 1980). We have $C^{34}S$ (1–0) and $C^{34}S$ (2–1) data obtained toward the CS (1–0) intensity maxima of some of the identified cores (Tatematsu et al. 1993). These data show that for $\sim$75% of the observed cores $\tau(C^{34}S\ 1\text{–}0)$ is less than 0.05, which corresponds to $\tau(CS\ 1\text{–}0) \leq 1$ if we assume the terrestrial isotopic ratio. The results are not affected by this moderate optical depth of the CS (1–0) line. Indeed, the CS (1–0) line width is quite close to the line width of the optically thin $C^{18}O$ line (from Table 2) as $\Delta v(CS\ 1\text{–}0) = (1.06 \pm 0.17)\Delta v(C^{18}O)^{0.93\pm0.21}$.

In a crowded region like the one discussed here, the error pattern of the telescope beam might affect the observed intensity distribution. This is not the case for our CS (1–0) results. The beam efficiency at the CS (1–0) frequency is as high as 0.6, and the clumpy CS emission will not have a very large filling factor in the error pattern. Furthermore, we identify CS cores by using both spatial and velocity information on the CS emission. In general, cores have different velocities. We think that contamination by other cores in the error beam is negligible for CS (1–0). For ^{13}CO, the beam efficiency of the telescope is lower (0.38), and the ^{13}CO line width is in general broader. It is possible that contamination due to the error pattern of the telescope affects the ^{13}CO intensity of weak cores located in or near the intense ^{13}CO ridge. However, the number of cores which can be affected by the error pattern contamination is not large (about 10). Among the physical parameters of the cores, only the core mass was derived by the aid of the ^{13}CO data. Only the results shown in § 3.1 and discussion based on the core mass might be partly affected by the error beam in a way that masses of $\sim$10 cores toward the low end of the mass spectrum are slightly ($\lesssim$30%) overestimated.

In § 3.1 we noted that the Orion A cloud shows 1 pc–sized clumps based on the ^{13}CO map. The cores identified from the CS (1–0) map and listed in Table 1 are much smaller (size $\sim$0.3 pc) and could belong to a subclass of clumps in the hierarchical nature of interstellar medium (see Scalo 1985). The number of cores contained within each of the four clumps ranges from 2 to 7, and the total mass of 18 molecular cores included in these four clumps is 2300 $M_\odot$: the CS (1–0) observation detects about 60% of the gas observed in ^{13}CO. The total mass of the 125 cores cataloged in the present study is 1.8×10^4 $M_\odot$. Maddalena et al. (1986) estimated the total mass of the Orion A giant molecular cloud to be of order 1×10^5 $M_\odot$ on the basis of their ^{12}CO observation. Because we did not fully cover the Orion A cloud, we can set a lower limit on the percentage of the mass involved in molecular cloud cores to about 20%. The lifetime of giant molecular clouds is of order 3×10^7 yr (e.g., Bash, Green, & Peters 1977; Turner 1988). If the lifetime of cores is several times the free-fall time (i.e., 10^5–10^6 yr) and

TABLE 3

PARAMETERS OF MOLECULAR CLOUD CORES

SAMPLE	LINE	R (pc)	Δv (km s^{-1}) All	Δv (km s^{-1}) No YSO[d]	log ($M/M_\odot$)	log ($M_{vir}/M_\odot$)
Orion A cloud[a].....	CS (1–0)	0.16 ± 0.06 (125)	1.21 ± 0.46 (125)	1.15 ± 0.38 (108)	1.9 ± 0.5 (125)[e]	1.6 ± 0.4 (125)
	CS (2–1)	...	1.90 ± 0.72 (21)	1.72 ± 0.45 (19)	...	...
	$C^{18}O$ (1–0)	...	1.68 ± 0.61 (14)	1.58 ± 0.50 (13)	...	...
Dark clouds	CS (2–1)[b]	0.14 ± 0.08 (10)	0.68 ± 0.25 (12)	0.52 ± 0.19 (4)	...	1.0 ± 0.5 (10)
	CS (3–2)[b]		0.68 ± 0.29 (22)	0.54 ± 0.14 (12)		
	$C^{18}O$ (1–0)[c]	...	0.63 ± 0.31 (70)	...	...	...

NOTE.—The 1 σ deviation is listed. The number of cores is shown in parentheses.

[a] Present work.

[b] Taken from Zhou et al. 1989. The bright-rimmed globule B35 is excluded.

[c] Myers, Linke, & Benson 1983.

[d] For Orion, cores without molecular outflows/cold *IRAS* sources. For dark clouds, cores associated with neither an *IRAS* point source nor a 2 μm source; no molecular outflow source is included in this category (Myers et al. 1988).

[e] From the integrated CS (1–0) intensity.

the percentage of the mass of cores does not vary very much during the lifetime of a giant molecular cloud, the remnant of cores will be repeatedly used to form next-generation cores.

4.2. *The Shape of the Cores*

The identified molecular cloud cores are mostly elongated. Four linear extents (FWHM in T_A^*) on the P-V diagrams for each core are used to derive the axial ratio and the position angle of the elongation. We calculated the axial ratio and position angle by fitting the four linear extents to a cosine curve using a nonlinear least-squares program. The beam-corrected axial ratio is 0.5 ± 0.2 (average $\pm$ 1 σ deviation), which is comparable to the value of 0.4–0.5 for cores in dark clouds studied by Myers et al. (1991). To measure the position angle, we eliminated the cores whose axial ratios are greater than 0.65 because the position angle is often difficult to estimate precisely. Figure 7 shows the position-angle distribution for the three divided regions. It is found that the core elongation tends to be parallel to global elongation of the filamentary molecular cloud. In region I the cloud is elongated in the north-south direction, and the position-angle distribution of the core elongation has a dip at $\sim$90°. In region II the cloud is elongated in the northeast-southwest direction, and the position-angle distribution peaks at $\sim$120°. Although region III is somewhat complicated, one may see that the cloud has filaments elongated in the northwest-southeast direction as well as those elongated in northeast-southwest direction. We see two peaks in the position-angle histogram corresponding to these directions. As discussed by Myers et al. (1991), such elongation may represent prolate cloudlets rather than oblate ones. The alignment with respect to the global filamentary cloud structure might suggest that the elongation has been caused through gravitational instability for an equilibrium filamentary cloud (see § 3.1) and/or controlled by globally aligned magnetic fields.

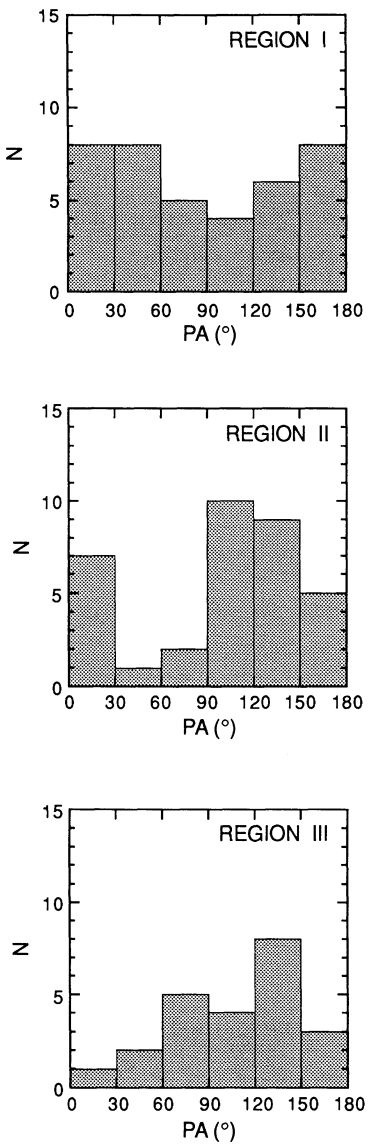

FIG. 7.—Distribution of the orientation of the core elongation for regions I, II, and III. Only the cores having axial ratios of $\leq$0.65 are plotted.

4.3. *Line Width, Core-to-Core Velocity Dispersion, and Mass of the Cores*

CS (2–1) spectra were obtained toward 21 out of the 125 Orion cores (Table 2). Figure 8 compares the CS (1–0) line width with the CS (2–1) line width for these 21 cores. No attempt was made to compensate for the difference in the beam size because the CS (2–1) observations were carried out solely toward the peak of the cores. The line width is roughly the same between these two transitions in Figure 8 except for a few sources (see also Linke & Goldsmith 1980 for a comparison of these two line widths for various sources).

Figure 9 compares the mass M ($M_\odot$) estimated from the integrated CS intensity with the CS (1–0) line width Δv (km s^{-1}). Using a nonlinear least-squares program, we obtained $\Delta v(\text{km s}^{-1}) = (0.43 \pm 0.05) M(M_\odot)^{0.23 \pm 0.02}$ (with 1 σ uncertainties). The correlation coefficient is 0.63. The present fit is consistent with the relation $\sigma(\text{km s}^{-1}) = 0.42 M(M_\odot)^{0.20}$ found by Larson (1981) for a large variety of regions (his σ is the three-dimensional velocity dispersion, and $\Delta v = 1.36\,\sigma$ for an optically thin Gaussian-shaped profile). Bally et al. (1987) obtained a similar relationship, $\Delta v(\text{km s}^{-1}) = 0.54 M(M_\odot)^{0.25}$, for 14 ^{13}CO clumps, which are larger in size and less dense

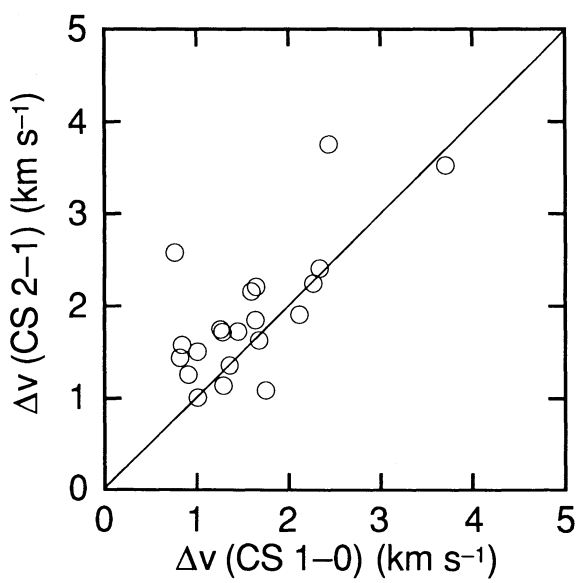

FIG. 8.—Relation between CS (1–0) and CS (2–1) line widths for 21 molecular cloud cores.

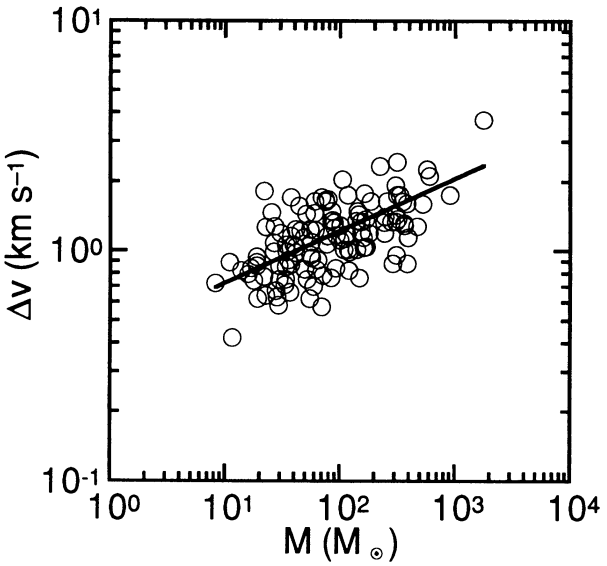

FIG. 9.—Relation between the core mass estimated from the integrated CS (1–0) intensity, and the CS (1–0) line width. The straight line represents the best fit, $\Delta v(\mathrm{km\ s^{-1}}) = 0.43 M(M_\odot)^{0.23}$.

than molecular cloud cores, found in the Orion A cloud. The correlation between the radius R and the line width Δv is not clear in our Orion sample, probably because the range of R obtained in the present identification is narrow.

We investigate the core-to-core velocity dispersion $\sigma_{c\text{-}c}$. It is known that the Orion A cloud has a global velocity gradient along the filament, whose direction (northwest-southeast) is nearly parallel to the Galactic longitude (Kutner et al. 1977). By using a linear least-squares program for the radial velocity of the cataloged cores versus the Galactic longitude, we obtained the relationship $V_{\mathrm{LSR}}(\mathrm{km\ s^{-1}}) = 7.70 - 1.994(l - 210°)$. The velocity gradient along the filament is of order 0.26 km s^{-1} pc^{-1} (cf. 0.135 km s^{-1} pc^{-1} by Kutner et al. 1977 for a larger area of the Orion A cloud). The velocity gradient across the filament (§ 3.1) was not corrected to derive $\sigma_{c\text{-}c}$ because the amount of this velocity gradient is not easy to derive precisely. The line-of-sight dispersion of the radial velocity of the cores $\sigma_{c\text{-}c}$ is estimated to be 1.15 km s^{-1}. This value is comparable to the ^{13}CO line width ($\sigma = 1.1 \pm 0.1$ km s^{-1}, FWHM $= 2.6 \pm 0.2$ km s^{-1}).

Last, we compare the mass obtained from the integrated CS (1–0) intensity M with the virial mass M_{vir}. Figure 10 illustrates M_{vir}/M as a function of M. It is remarkable that M_{vir}/M is not constant but is correlated with M. Using a nonlinear least-squares program, we can obtain $M_{\mathrm{vir}}/M = (2.8 \pm 0.6) M(M_\odot)^{-0.35 \pm 0.05}$ with a correlation coefficient of 0.55. A similar result was previously obtained by Loren (1989) for ^{13}CO clumps in the ρ Oph molecular cloud: $M_{\mathrm{vir}}/M \propto M^{-0.61}$. It should be noted that the power for his ^{13}CO clumps (−0.61) is much steeper than that for our Orion data (−0.35). He concluded that low-mass clumps deviate from virial equilibrium ($M_{\mathrm{vir}} > M$). Because our estimates of M depend on the CS abundance, which can differ by a factor of 5 from the adopted value, we cannot determined which of the massive cores and low-mass cores are close to virial equilibrium in our sample. At least the variation of log (M_{vir}/M) of the cores in Orion (1 σ deviation is 0.29) is much less than that of Loren's ^{13}CO clumps in ρ Oph, and we guess that all cores in our sample are not far from virial equilibrium.

4.4. *Association of Cores with Young Stellar Objects*

Next, we investigate the percentage of the cores accompanying young stellar objects. Molecular outflows indicate the presence of YSOs. There exist 12 molecular outflows within the mapped regions (Lada 1985 and references therein; Fukui 1989 and references therein; Ziurys et al. 1990; Morgan et al. 1991). Eleven of the 12 outflows (92%) are located within the half-intensity contour of the identified molecular cloud cores. In other words, 9% of the 125 cores are found to be associated with molecular outflows. YSOs are generally observed as cold-color *IRAS* point sources [log ($F_\nu^{12\,\mu\mathrm{m}}/F_\nu^{25\,\mu\mathrm{m}}$) ≤ 0] (see Fukui et al. 1989; Morgan & Bally 1991). When we include cold *IRAS* point sources located within cores (half-intensity level) as YSO candidates, the number of the cores accompanying YSOs or YSO candidates is 17. We list molecular outflows and cold *IRAS* point sources apparently associated with the identified cores in Table 1. The identification of *IRAS* point sources in L1641 (the southern portion of the Orion A cloud) is summarized in Strom et al. (1989). Cores associated with YSOs (including candidates) tend to have slightly larger CS (1–0) line width (1.58 ± 0.67 km s^{-1}; average $\pm$ 1 σ deviation) than those without YSOs (1.15 ± 0.38 km s^{-1}). This result is consistent with those derived by Beichman et al. (1986), Myers et al. (1988), and Zhou et al. (1989). Because the Orion Nebula region is heavily confused by diffuse infrared emission, elimination of cores at decl. $> -6°$ might provide better statistics for YSO-core association. In this case, 12% (8/68) of the cores accompany outflows, and 18% (12/68) of the cores accompany outflows and/or cold *IRAS* sources.

In our sample, 10%–20% of the cataloged cores are found to accompany YSOs or YSO candidates. This value is much lower than the value of 50%–70% for NH_3 cores in dark clouds studied by Benson & Myers (1989). We discuss a few points which may affect statistics. First, this difference in percentage would be likely due to a higher detection limit for YSOs in Orion because the Orion A cloud is more distant and more confused by diffuse infrared emission than nearby dark

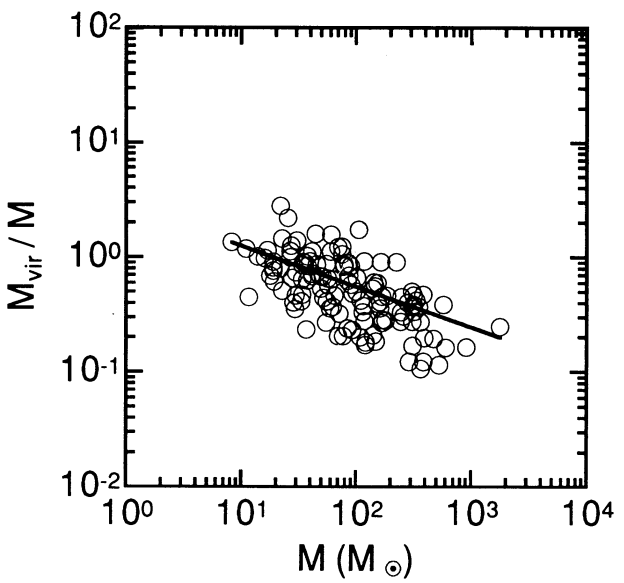

FIG. 10.—Ratio of the virial mass M_{vir} to the mass M obtained from the integrated CS (1–0) intensity is shown as a function of M. The straight line represents the best fit, $M_{\mathrm{vir}}/M = 2.8 M(M_\odot)^{-0.35}$.

clouds. For example, we look into the detection limit of the *IRAS* Point Source Catalog. Wilking, Lada, & Young (1989) and Kenyon et al. (1990) obtained luminosity functions for the Ophiuchus and Taurus-Auriga regions, respectively. The detection limit of the *IRAS* Point Source Catalog is about 0.5 $L_\odot$ at the distance to these regions (150 pc). Because the Orion A cloud is 3 times as distant, the detection limit is about 5 $L_\odot$. Although the luminosity function of *IRAS* point sources in Orion might differ from those in these two regions, we simply count the number of both class I and II sources and derive the percentage of sources whose luminosity is greater than 5 $L_\odot$. This percentage is 26% for Ophiuchus and 22% for Taurus-Auriga. Second, it is also possible that the detection limit of our survey might be higher than that in studies of dark cloud cores. It is more difficult to assess the difference in detection limit because different telescopes and different lines are used. When we compare the linear size of the telescope beam, our beam size, 0.08 pc, is comparable to those used by Benson & Myers (1989), 0.05 pc (National Radio Astronomy Observatory 43 m telescope) and 0.06 pc (Haystack 37 m telescope). Therefore, we think the difference in the detection limit for the cores is smaller than that for YSOs. Last, it is possible that our survey has detected cores prior to star formation more efficiently than their NH_3 observations, as we discussed in § 3.2. In reality the abundance of NH_3 is often enhanced toward star-forming regions (e.g., Suzuki et al. 1992).

The statistics of the fraction of star-forming cores will be interesting in the context of the core evolution leading to star formation, although the present study is still not enough for this purpose. Because the molecular cloud core is close to virial equilibrium, the time scale of the core evolution might be several times the free-fall time scale (i.e., 10^5–10^6 yr). On the other hand, the time scales for molecular outflows and embedded YSOs might be 10^4–10^5 and 10^5 yr, respectively (e.g., Lada 1985; Kenyon et al. 1990). The ratio of these time scales is roughly consistent with the fraction of cores (10%–20%) which have already formed stars. We also wonder whether all cores eventually lead to star formation. Further studies, especially sensitive surveys of YSOs in Orion, are highly desirable.

4.5. *Alternative Core Identification Levels*

The physical parameters of molecular cloud cores may vary when the procedure of core identification is changed. When we only use 65 cores whose peak CS intensities are larger than 2.38 K (7 σ) out of the 125 cores (with the original threshold of 5 σ), the mean properties of the cores in CS (1–0) become $R = 0.17 \pm 0.06$ pc, $\Delta v = 1.24 \pm 0.53$ km s^{-1}, $\log (M/M_\odot) = 2.1 \pm 0.4$, and $\log (M_{\rm vir}/M_\odot) = 1.6 \pm 0.4$. The parameters from the 7 σ criterion are very similar to those listed in Table 3, except $\log (M/M_\odot)$, which slightly increases.

One could identify cores by using separation at the half-intensity level instead of a fixed threshold. We test this identification by using the 125 cores listed in Table 1 as candidates. We identify 52 cores from the test identification. For example, core 31 (Orion-S) is involved in core 29 (Orion KL). The mean properties of the cores become $R = 0.20 \pm 0.07$ pc, $\Delta v = 1.20 \pm 0.51$ km s^{-1}, $\log (M/M_\odot) = 2.1 \pm 0.6$, and $\log (M_{\rm vir}/M_\odot) = 1.7 \pm 0.4$. We obtained somewhat larger average radius, core mass, and virial mass. Results from this test identification are not very different from those from the original identification. For example, we obtain a similar Δv-M relation: Δv(km s^{-1}) = $(0.35 \pm 0.06) M(M_\odot)^{0.25 \pm 0.03}$.

We think that the results in the present study do not strongly depend on how we identify molecular cloud cores (see also § 6).

5. COMPARISON OF THE CORES

5.1. *Comparison with Cores in Dark Clouds*

It has been suggested that the mass of stars being formed in the Orion molecular cloud is systematically larger than that of stars being formed in dark clouds such as the Taurus dark clouds (e.g., Cohen & Kuhi 1970; Larson 1982). The difference in the stellar mass must reflect the difference in the physical parameters of molecular cloud cores from which stars form. To investigate this issue, it would be important to compare the characteristic parameters of the cores estimated above with those of cores in dark clouds.

Table 3 summarizes a comparison of the physical properties for the cores in the Orion A cloud with those estimated for cores in dark clouds by Zhou et al. (1989). Zhou et al. studied 27 molecular cloud cores in nearby dark clouds by observing CS (2–1) with the 12 m radio telescope of the National Radio Astronomy Observatory (NRAO) at Kitt Peak and/or CS (3–2) with the 4.9 m radio telescope of the Millimeter Wave Observatory (MWO) in Texas. The beam sizes they employed (1′ for CS 2–1 and 1′.6 for CS 3–2) correspond to 0.04 and 0.07 pc at the typical distance, $\sim$150 pc, to the objects they observed. These values are smaller than, by a factor of 2, and similar to our beam size (0.08 pc at a distance of 450 pc). The cores observed are partly associated with YSOs and partly without YSOs.

First, we compare the radii of the cores. The size R defined by Zhou et al. (and by Myers et al. 1983) is twice the radius R in our definition, and we have translated their size R to match our definition. The radius of the cores in Orion, 0.16 ± 0.06 pc, is comparable to that in dark clouds, 0.14 ± 0.08 pc.

Second, we compare the line widths. It is remarkable that the line width of the molecular cloud cores in the Orion A cloud is broader by a factor of 2 than that of the cores in dark clouds (Table 3). Although the data on dark cloud cores by Zhou et al. (1989) do not include CS (1–0), which we observed, the data assembled in Table 3 clearly show this tendency. Note that in the sample of Zhou et al. the CS (2–1) line width is nearly equal to the CS (3–2) line width (see their Fig. 2), and in our sample the CS (1–0) line width is nearly equal to the CS (2–1) line width (Fig. 8). Figure 11 shows the line-width distribution in Orion and in dark clouds. The line width for the Orion molecular cloud cores is 1–3 km s^{-1} for CS (1–0) and CS (2–1), and is broader than the CS (2–1) line width ($\lesssim$1 km s^{-1}) for the cores in dark clouds. The difference in line-width distribution between CS (1–0) and CS (2–1) in Orion (Fig. 11) is mainly due to a fact that the 21 cores observed in CS (2–1) are not randomly selected but are chosen from the northern portion of the surveyed region (see § 5.2 and Fig. 8).

As a natural consequence of similar core size and larger line width, the virial mass of the Orion molecular cloud cores is, as an ensemble, larger than that of the cores in dark clouds as shown in Table 3.

On the basis of NH_3 observations toward *IRAS* point sources, Wouterloot, Walmsley, & Henkel (1988) found that the NH_3 (1, 1) line width in Orion is larger than that in nearby dark clouds (see also Harju, Walmsley, & Wouterloot 1991). A molecular cloud core with an embedded young stellar object (YSO) shows a broader line width than that without a YSO

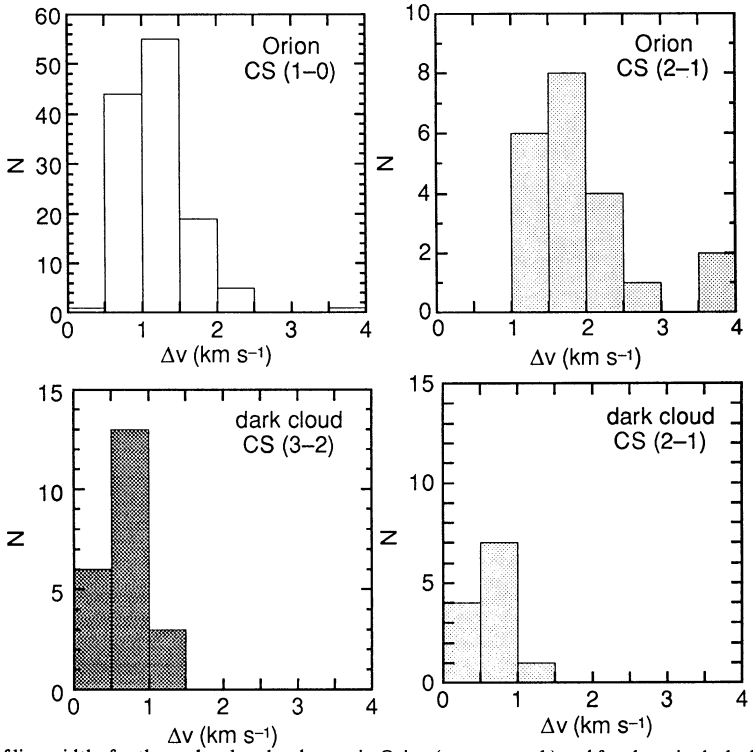

FIG. 11.—Histograms of line widths for the molecular cloud cores in Orion (present work) and for those in dark clouds (Zhou et al. 1989)

(Beichman et al. 1986; Myers et al. 1988; Zhou et al. 1989; present work). Because our sample contains cores both with and without YSOs, it may give us a better sample to estimate the intrinsic properties of the molecular cloud cores, which can be directly compared with the sample in dark clouds containing cores with and without YSOs. Our conclusion that the line width is larger for the Orion molecular cloud cores is found to hold whether we include or exclude the cores with the YSOs (Table 3).

We have seen that the Orion cores have larger line widths than the dark cloud cores, although the core radii are similar. We may overlook cores having narrow line width, because we used 0.5 km s^{-1} interval channel maps in the identification procedure. The deficiency of cores having narrow line width $\Delta v \lesssim 1$ km s^{-1} might be due to the detection limit (see § 6 for further discussion). To know the meaning of larger line width observed in Orion, we consider the Δv-R correlation, which is one of the important characteristics of molecular cloud cores (e.g., Chièze 1987; Myers & Goodman 1988; Fuller & Myers 1992; Myers & Fuller 1992). Compared with other physical parameters such as the core mass, these two parameters are much more reliable because they are directly derived from the observations. The radius range of our Orion sample is too narrow to derive the relation independently. The Δv-R relation for the dark cloud cores is given by Fuller & Myers (1992) on the basis of the NH_3, CS (2–1), and $C^{18}O$ (1–0) data: $\log \Delta v = (0.44 \pm 0.08) \log R + (0.01 \pm 0.08)$ (for cores without YSOs). Here R is in parsecs and Δv is in kilometers per second. This linear relation can be translated into $\Delta v(\text{km s}^{-1}) = 1.02R(\text{pc})^{0.44}$. The CS (2–1) data they used are basically identical to those of Zhou et al. (1989). On the other hand, the Orion cores rather obey the relation Δv (km s^{-1}) = $1.95R(\text{pc})^{0.38}$, obtained by Larson (1981). $C^{18}O$ cores in the M17 SW region studied by Stutzki & Güsten (1990) also seem to follow Larson's relation rather than that of Fuller & Myers (1992). Because our sample is too narrow in radius range to derive the power, we estimate only the coefficient A by assuming the relation $\Delta v(\text{km s}^{-1}) = AR(\text{pc})^{0.4}$. The power 0.4 is assumed on the basis of the estimates by Larson (1981) and by Fuller & Myers (1992). The least-squares fitting to the Orion cores gives $A = 2.5 \pm 0.1$, whereas that to the dark cloud cores of Zhou et al. (1989) provides $A = 1.5 \pm 0.1$. Here we include cores both with and without YSOs. The errors reflect only 1 σ uncertainties in fitting. It seems that the Δv-R relation differs between the cores in giant molecular clouds (Orion and M17 SW) and those in dark clouds (see § 7). Larson (1981) pointed out that the Δv-R relation seems to differ among different clouds (see his Fig. 2).

Figure 12 shows a Δv-R plot for the cores without YSOs in Orion and those in dark clouds. According to Fuller & Myers, there is significantly less scatter in the Δv-R correlation for cores without YSOs than that for cores with YSOs. Harju et al. (1991) mapped NH_3 toward *IRAS* point sources in Orion. Eight of the 26 NH_3 cores they detected are thought not to be associated with the *IRAS* point sources, and we include them in Figure 12. The NH_3 line is optically thin. Harju et al. (1991) did not list the line width for each NH_3 core. If we plot each of the 108 CS cores without YSOs, the plot becomes too crowded. Therefore, the average and 1 σ deviation are shown for the cores in Orion, whereas the cores in dark clouds taken from Fuller & Myers (1992) are plotted for each core. It is clearly shown that the cores in Orion are located above the best fit for dark cloud cores on the Δv-R plot.

5.2. *Spatial Difference of Core Properties within the Orion A Cloud*

We compare core properties in different regions in the Orion A giant molecular cloud. We divide the survey areas into three

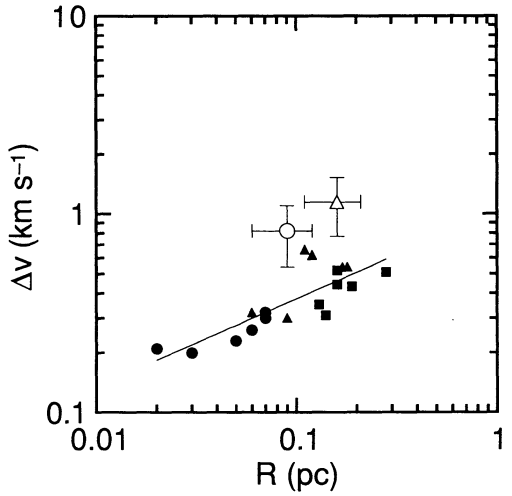

FIG. 12.—Δv-R plot for the cores without YSOs in Orion (*open triangle:* CS 1–0, present study; *open circle:* NH_3, Harju, Walmsley, & Wouterloot 1991) and those in dark clouds (*filled triangles:* CS 2–1, *filled circles:* NH_3, *filled squares:* $C^{18}O$, Fuller & Myers 1992). The straight line represents the best fit for the cores in dark clouds.

regions such that each region has similar length along the ridge of the Orion A cloud: region I ($-4°55' >$ decl. $\geq -5°50'$) containing the Orion Nebula, region II ($-5°50' >$ decl. $\geq -6°55'$), and region III ($-6°55' >$ decl. $\geq -7°40'$). The areas of regions I, II, and III are 613, 980, and 921 arcmin^2, and the numbers of cores in the three regions are 52, 42, and 31, respectively. In the Orion A cloud, massive stars tend to be located in the northern part. It would be interesting to know whether the core properties vary with the position along the filament or not.

Figure 13 shows the distributions of the line width and mass of the molecular cloud core for the three regions. As seen from this figure, the width and mass of the cores tend to be larger toward the north. Even in region III, the line width is somewhat larger than that in dark clouds. Table 4 summarizes several parameters for the three regions. The average density and core-to-core velocity dispersion $\sigma_{c\text{-}c}$ show a tendency similar to the CS line width of the cores. From the present results, we conclude that the core properties vary from the north to the south in the Orion A cloud.

The average core radius R differs slightly among the three regions. In region II, R shows the largest average value. For the three regions, we estimate the coefficient of the Δv-R relation by assuming the form $\Delta v(\mathrm{km\ s^{-1}}) = AR(\mathrm{pc})^{0.4}$. The value of A is estimated to be 2.9 ± 0.2, 2.3 ± 0.1, and 2.2 ± 0.1, for regions I, II, and III, respectively (with 1 σ uncertainties in fitting). The coefficient is larger toward the north. The coefficient for

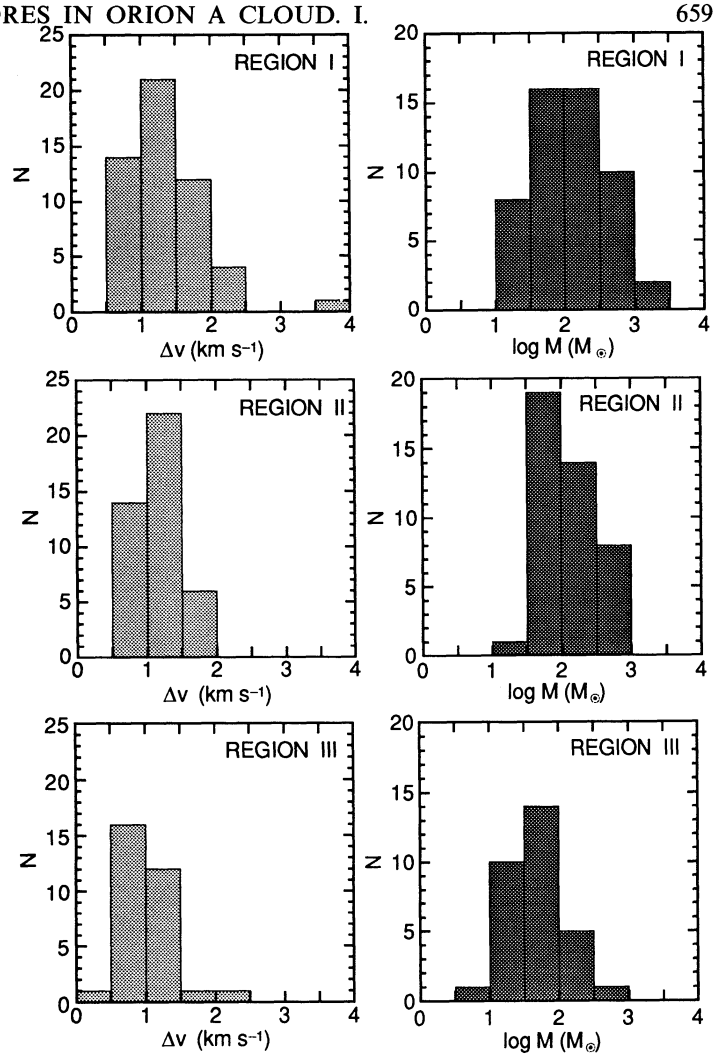

FIG. 13.—Comparisons of the line widths and masses of cores among regions I, II, and III of the Orion A cloud.

regions II and III is 1.6 times larger than the value of 1.5 ± 0.1 obtained for the dark cloud cores of Zhou et al. (1989). The cores in region I have smaller R and larger A possibly because of larger external pressure by ionized gas of the Orion Nebula (see § 7).

6. MASS SPECTRUM OF THE CORES AND THE DETECTION LIMIT IN OUR SURVEY

We deduced the mass spectrum of the molecular cloud cores found in the Orion A cloud (Fig. 14). By using a linear least-squares program, the mass spectrum can be fitted by log (dN/

TABLE 4

COMPARISON OF REGIONS I, II, AND III

	R (pc)		Δv (km s^{-1})		$\sigma_{c\text{-}c}$ (km s^{-1})		log [n(cm^{-3})][a]		log ($M/M_\odot$)	
REGION	All	No YSO	All	No YSO	All	No YSO	All	No YSO	All	No YSO
I.....	0.14 ± 0.05	0.15 ± 0.05	1.34 ± 0.55	1.28 ± 0.43	1.35	1.29	5.2 ± 0.4	5.2 ± 0.4	2.0 ± 0.5	2.0 ± 0.5
II.....	0.19 ± 0.06	0.19 ± 0.06	1.15 ± 0.34	1.11 ± 0.32	1.00	0.99	4.9 ± 0.2	4.8 ± 0.2	2.0 ± 0.4	1.9 ± 0.4
III.....	0.16 ± 0.04	0.16 ± 0.04	1.06 ± 0.36	0.95 ± 0.29	0.91	0.91	4.7 ± 0.2	4.6 ± 0.2	1.6 ± 0.4	1.6 ± 0.4

NOTE.—The 1 σ deviation is listed.

[a] $n = 1.2\, n(H_2) = 0.6\, N(H_2)/R$.

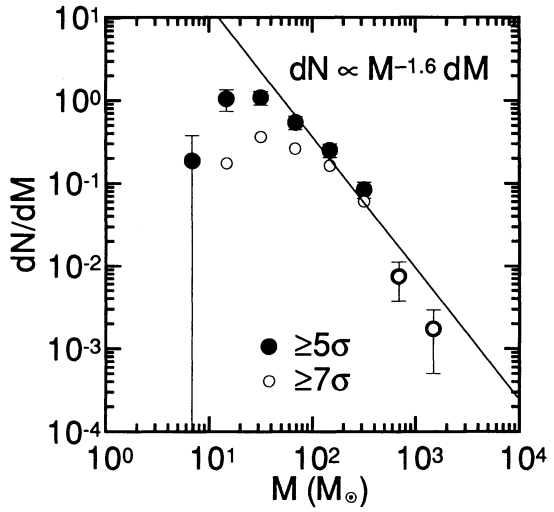

FIG. 14.—Mass spectra of the Orion molecular cloud cores. Large filled circles represent the spectrum obtained with the 5 σ criterion for core identification, whereas small open circles represent that obtained with the 7 σ criterion. The error bars reflect only $N^{1/2}$ counting uncertainties. The straight line $dN \propto M^{-1.6}\,dM$ represents the best fit for the core mass range log $M(M_\odot) \geq 1.67$ (or $M \gtrsim 50\ M_\odot$).

$dM) \propto \gamma$ log M with $\gamma = -1.6 \pm 0.3$ for log $M(M_\odot) \geq 1.67$ (or $M \gtrsim 50\ M_\odot$). The index γ is -1.2 ± 0.1 for the different core mass range log $M(M_\odot) = 1.67$–2.67, and $\gamma = -2.0 \pm 0.3$ for log $M(M_\odot) \geq 2$. It seems that the mass spectrum becomes steep with increasing core mass. When we used the 52 cores from the test identification at the half-intensity level (§ 4.5), we obtain $\gamma = -1.5 \pm 0.2$ for the mass range log $M(M_\odot) \geq 1.67$. Scalo (1985) reviews previous estimates of the mass spectrum index. From the NH_3 data of Benson & Myers (1989), Scalo (1985) obtained the mass spectrum index for dark cloud cores to be $\gamma = -1.5$ to -1.0 for $M \geq 4\ M_\odot$. The index obtained here is close to $\gamma = -1.7$ for $M \geq 10\ M_\odot$ obtained by Stutzki & Güsten (1990) for the M17 SW region.

Below 30 $M_\odot$, the mass spectrum becomes flat, probably because of the incompleteness of our survey. We may overlook smaller ($R < 0.1$ pc) cores because of the limited spatial resolution (0.08 pc HPBW), cores with lower intensities because of the limited sensitivity (5 σ = 1.7 K) and confusion, and cores having narrow line width in the identification procedure. If we use the relation Δv(km s^{-1}) = $2.5R$(pc)$^{0.4}$, the detection limit $R = 0.1$ pc corresponds to $\Delta v = 1$ km s^{-1}. On the other hand, for core identification, we used 0.5 km s^{-1} interval channel maps and 0.3 km s^{-1} resolution P-V diagrams, and cores with a line width of $\leq$0.5 km s^{-1} can be overlooked in our procedure. Here we use 1 km s^{-1} for the detection limit in the line width. From the best-fit relation between the CS line width and the core mass, i.e., Δv(km s^{-1}) = $0.43M(M_\odot)^{0.23}$, the limit $\Delta v = 1$ km s^{-1} corresponds to 40 $M_\odot$. This probably explains the turnover. Figure 14 also shows how the spectrum would look when the criterion for the identification of cores was increased to the 7 σ level (§ 4.5). The expected detection limit for the 7 σ mass spectrum is $\sim$50 $M_\odot$, whereas the turnover is seen at $\sim$100 $M_\odot$. When we take into account the error in mass estimation (a factor of $\sim$4 judging from the correlation for M_{vir} versus M), the turnover is likely to mean the survey detection limit. The statistics of the high-mass cores ($M \gtrsim 50\ M_\odot$) are not affected heavily by this detection limit, and we can definitely state that in the Orion A cloud there are molecular cloud cores having large line width and mass, which are rarely seen in dark clouds.

7. DISCUSSION

7.1. *Mass Spectrum of the Cores and the Initial Mass Function*

The mass spectrum of molecular cloud cores, which are in the intermediary stage in the cloud evolution toward star formation, is important because it can be related to the stellar initial mass function (IMF). Salpeter's (1955) power-law IMF with an index -2.35 is much steeper than the mass spectrum of molecular cloud cores with an index -1.6 which we have obtained for the Orion A cloud. Zinnecker (1990; see also Stutzki & Güsten 1990) discussed the relationship among the mass spectrum of clumps, the stellar IMF, and subfragmentation in clumps. In the context of the present paper, his "clumps" may read "molecular cloud cores." He pointed out a possibility that the IMF might be related to the mass spectrum of cores through star formation efficiency, or the relation between the core mass M and the mass M_* of a star born in the core. Larson (1982) obtained an empirical relation between the cloud mass and the maximum stellar mass, whereas Nakano (1984) numerically investigated a relation between the mass of a magnetic cloud and that of gas which finally contracts dynamically. From these results we assume $M_* \propto M^{0.4}$. The spectrum $dN/dM \propto M^\gamma$ for cores is translated into the IMF $dN_*/dM_* \propto M_*^{-1+(\gamma+1)/0.4}$. For $\gamma = -1.6$ we obtain -2.5 for the index of the IMF, which is close to Salpeter's IMF index -2.35. In this discussion we have ignored multiple star formation from one core (Tatematsu & Umemoto 1991).

7.2. *Difference in the Core Properties and Its Implications for Star Formation*

Why can giant molecular clouds form massive stars? It is known that the total masses of giant molecular clouds are two orders of magnitude larger than those of dark clouds. We found many molecular cloud cores in the Orion A giant molecular cloud, and it seems that giant molecular clouds contain more numerous cores than dark clouds. The mass spectrum index for the Orion cores is not greatly different from that for dark cloud cores, although the line observed is different in the two samples. Because the giant molecular cloud is more massive, the number of massive cores would be much larger in the Orion A cloud even though the mass spectrum index is similar. It seems that the giant molecular cloud contains (more) massive cores mainly because the total number of cores within it is large. One may think that massive cores have the potential of producing massive stars because cores have a larger amount of material which can fall onto protostars.

We wonder whether the difference in the mass of stars being formed between giant molecular clouds and dark clouds can be explained only in terms of the difference in the number of cores. We suggested in § 5.1 that the Δv-R relation differs between cores in the Orion A giant molecular cloud and those in dark clouds. The Δv-R relation will vary when external pressure (Chièze 1987; Maloney 1988) or the strength of magnetic fields (Myers & Goodman 1988) changes.

It is important that giant molecular clouds have the advantage of keeping turbulent less dense gas within their deep gravitational potential because they are more massive than dark clouds. Furthermore, giant molecular clouds have a larger possibility of experiencing events which will fill up this deeper gravitational potential with high-pressure (turbulent) gas:

winds from numerous young stellar objects within them (Norman & Silk 1980), associated H II regions, and external compression by superbubbles, which might be originated from old OB associations. By following the argument of Chièze (1987), the difference in the coefficient for the Δv-R relation shown in § 5.1 might suggest that the external gas pressure for the cores in the Orion A cloud is roughly one order of magnitude larger than that for the dark cloud cores. Bally et al. (1987) suggested from their data that the Orion A cloud has been compressed by a superbubble (see also an illustration shown by Jenniskens & Wouterloot 1990). The northern part has been compressed earlier and more strongly because it is closer to the center of expansion. This is one of the possible explanations for the change we have found in the core properties within the Orion A cloud. In the northern part the cores have larger line width, larger average density, and a larger coefficient for the Δv-R relation. In addition, in a part of region I, the core properties might be influenced by the presence of the Orion Nebula, which probably have caused additional high external pressure for cores.

In general, the line width of less dense ($n \sim 10^2$–10^3 cm^{-3}) molecular gas traced by CO and ^{13}CO toward giant molecular clouds is broader (3–15 km s^{-1}) than that toward dark clouds (0.5–3 km s^{-1}) (e.g., Turner 1988). If, in giant molecular clouds, cores are generally embedded in high-pressure (turbulent) gas, we may observe the Δv-R relation with a larger coefficient. Another explanation is that cores in giant molecular clouds are supported by stronger magnetic fields. We suggest that cores in giant molecular clouds are bounded by high-pressure gas or are supported by stronger magnetic fields than cores in dark clouds.

We discuss the implications of different Δv-R relations for star formation. It is suggested that the mass infall rate is proportional to a^3, where a is the local effective sound speed which includes all mechanical supports such as turbulent motion and magnetic pressure (Shu 1977; Stahler, Shu, & Taam 1980). Here we attribute the observed line width to the local effective sound speed. On the basis of the same assumption, Heyer et al. (1986) investigated the relationship between the velocity dispersion of the cloud (core) with a YSO and the stellar luminosity. The present study clearly shows that the Orion A cloud contains many cores with internal velocity dispersion significantly larger than that in dark cloud cores, although the radius is similar. When we take Δv (FWHM) = 1.2 km s^{-1} for the cores found in Orion and 0.7 km s^{-1} for those in dark clouds, the mass-infall rate is of order 3×10^{-5} and 6×10^{-6} $M_\odot$ yr^{-1}, respectively. Molecular cloud cores with the large line widths commonly found in the Orion A giant molecular cloud would have high mass-infall rates onto protostars, which may lead to larger final stellar masses (Nakano 1989).

Although it may be premature to answer definitely the question "What governs the stellar mass?" we believe that the difference in core properties found in the present study gives an important clue to solving this long-standing problem.

8. SUMMARY

We have studied the Orion A giant molecular cloud through the CS (1–0) and ^{13}CO (1–0) observations by using the 45 m telescope of the Nobeyama Radio Observatory. The main results are summarized as follows:

1. We have identified 125 molecular cloud cores. The mean properties of the cores are HWHM radius 0.16 pc, line width 1.2 km s^{-1}, and mass 80 $M_\odot$. The average axial ratio of the cores is about 0.5, and their elongation tends to be parallel to the filamentary molecular cloud where they are embedded.
2. The CS line width of the molecular cloud cores in Orion is about twice as broad as that of dense cores in dark clouds, although there is no significant difference in size for these two samples. It is suggested that the Δv-R relation differs between these two samples.
3. Within the Orion A cloud, the CS line width, core mass, average density, and core-to-core velocity dispersion all tend to decrease toward the south.
4. The mass spectrum of the molecular cloud cores can be approximated by a power law $dN/dM \propto M^{-1.6}$ for the core mass range $M \gtrsim 50\ M_\odot$.
5. It is suggested that cores in giant molecular clouds are bounded by higher external pressure than those in dark clouds. Consequently, cores in giant molecular clouds have the potential of forming massive stars because of large internal velocity dispersion (FWHM line width $\gtrsim 1$ km s^{-1}), which is rare in dark cloud cores.

K. T. and T. U. wish to acknowledge N. Ukita for continuous encouragement during the course of the Orion survey, which was carried out as one of the NRO projects. The authors thank H. Chen, T. Hanawa, M. H. Heyer, F. Palla, J. Schmidt-Burgk, S. W. Stahler, K. M. Strom, S. E. Strom, Y. Uchida, S. Zhou, and H. Zinnecker for fruitful discussions.

REFERENCES

Bally, J., Langer, W. D., Stark, A. A., & Wilson, R. W. 1987, ApJ, 312, L45
Bash, F. N., Green, E., & Peters, W. L. 1977, ApJ, 217, 464
Bastien, P. 1983, A&A, 119, 109
Batrla, W., Wilson, T. L., Bastien, P., & Ruf, K. 1983, A&A, 128, 279
Beichman, C. A., Myers, P. C., Emerson, J. P., Harris, S., Mathieu, R., Benson, P. J., & Jennings, R. E. 1986, ApJ, 307, 337
Benson, P. J., & Myers, P. C. 1989, ApJS, 71, 89
Blake, G. A., Sutton, E. C., Masson, C. R., & Phillips, T. G. 1987, ApJ, 315, 621
Castets, A., Duvert, G., Dutrey, A., Bally, J., Langer, W. D., & Wilson, R. W. 1990, A&A, 234, 469
Chièze, J. P. 1987, A&A, 171, 225
Cohen, M., & Kuhi, L. V. 1979, ApJS, 41, 743
Dutrey, A., Langer, W. D., Bally, J., Duvert, G., Castets, A., & Wilson, R. W. 1991, A&A, 247, L9
Fukui, Y. 1989, in ESO Workshop on Low Mass Star Formation and Pre–Main Sequence Objects, ed. B. Reipurth (Garching: ESO), 95
Fukui, Y., Iwata, T., Takaba, H., Mizuno, A., Ogawa, H., Kawabata, K., & Sugitani, K. 1989, Nature, 342, 161
Fuller, G. A., & Myers, P. C. 1992, ApJ, 384, 523
Genzel, R., & Stutzki, R. 1989, ARA&A, 27, 41
Graedel, T. E., Langer, W. D., & Frerking, M. A. 1982, ApJS, 48, 321
Hanawa, T., et al. 1993, ApJ, submitted
Harju, J., Walmsley, C. M., & Wouterloot, J. G. A. 1991, A&A, 245, 643
Hasegawa, T. 1987, in IAU Symp. 115, Star Forming Regions, ed. M. Peimbert & J. Jugaku (Dordrecht: Reidel), 123
Herbst, E., & Leung, C. M. 1989, ApJS, 69, 271
Heyer, M. H., Snell, R. L., Goldsmith, P. F., Strom, S. E., & Strom, K. M. 1986, ApJ, 308, 134
Hirahara, Y., et al. 1992, ApJ, 395, 539
Jenniskens, P., & Wouterloot, J. G. A. 1990, A&A, 227, 553
Kenyon, S. J., Hartmann, L. W., Strom, K. M., & Strom, S. E. 1990, AJ, 99, 869
Kutner, M. L., Tucker, K. D., Chin, G., & Thaddeus, P. 1977, ApJ, 215, 521
Lada, C. J. 1985, ARA&A, 23, 267
Lada, E. A., Bally, J., & Stark, A. A. 1991, ApJ, 368, 432
Larson, R. B. 1981, MNRAS, 194, 809
———. 1982, MNRAS, 200, 159
———. 1985, MNRAS, 214, 379
Linke, R. A., & Goldsmith, P. F. 1980, ApJ, 235, 437
Little, L. T., MacDonald, G. H., Riley, P. W., & Matheson, D. N. 1979, MNRAS, 189, 539

Loren, R. B. 1989, ApJ, 338, 925
Maddalena, R. J., Morris, M., Moscowitz, J., & Thaddeus, P. 1986, ApJ, 303, 375
Maloney, P. 1988, ApJ, 334, 761
Morgan, J. A., & Bally, J. 1991, ApJ, 372, 505
Morgan, J. A., Schloerb, F. P., Snell, R. L., & Bally, J. 1991, ApJ, 376, 618
Myers, P. C. 1983, ApJ, 270, 105
Myers, P. C., & Benson, P. J. 1983, ApJ, 266, 309
Myers, P. C., & Fuller, G. A. 1992, ApJ, 396, 631
Myers, P. C., Fuller, G. A., Goodman, A. A., & Benson, P. J. 1991, ApJ, 376, 561
Myers, P. C., & Goodman, A. A. 1988, ApJ, 329, 392
Myers, P. C., Heyer, M., Snell, R. L., & Goldsmith, P. F. 1988, ApJ, 324, 907
Myers, P. C., Linke, R. A., & Benson, P. J. 1983, ApJ, 264, 517
Nakano, T. 1984, Fund. Cosmic Phys., 9, 139
———. 1989, ApJ, 345, 464
Norman, C. A., & Silk, J. 1980, ApJ, 238, 158
Salpeter, E. E. 1955, ApJ, 121, 161
Scalo, J. M. 1985, in Protostars & Planets II, ed. D. C. Black & M. S. Matthews (Tucson: Univ. Arizona Press), 201
Schloerb, F. P., & Loren, R. B. 1982, in Symposium on the Orion Nebula to Honor Henry Draper, ed. A. E. Glassgold, P. J. Huggins, & E. L. Schucking (New York: NY Acad. Sci.), 32
Schmidt-Burgk, J., Güsten, R., Mauersberger, R., Schulz, A., & Wilson, T. L. 1990, ApJ, 362, L25
Shu, F. H. 1977, ApJ, 214, 488
Snell, R. L., Langer, W. D., & Frerking, M. A. 1982, ApJ, 255, 149
Stahler, S. W., Shu, F. H., & Taam, R. E. 1980, ApJ, 241, 637
Strom, K. M., Newton, G., Strom, S. E., Seaman, R. L., Carrasco, L., Cruz-Gonzalez, I., & Serrano, A. 1989, ApJS, 71, 183
Stutzki, J., & Güsten, R. 1990, ApJ, 356, 513
Suzuki, H., Yamamoto, S., Ohishi, M., Kaifu, N., Ishikawa, S., Hirahara, Y., & Takano, S. 1992, ApJ, 392, 551
Swade, D. A. 1989, ApJ, 345, 828
Tatematsu, K., et al. 1993, in preparation
Tatematsu, K., & Umemoto, T. 1991, Mem. Soc. Astron. Italiana, 62, 813
Tsuboi, M. 1991, in The 1991 Microwave Workshops and Exhibition (Tokyo: IEICE), 303
Turner, B. E. 1988, in Galactic and Extragalactic Radio Astronomy, ed. G. L. Verschuur & K. I. Kellermann (2d ed.; New York: Springer-Verlag), 154
Uchida, Y., Fukui, Y., Minoshima, Y., Mizuno, A., Iwata, T., & Takaba, H. 1991, Nature, 349, 140
Ulich, B. L., & Haas, R. W. 1976, ApJS, 30, 247
Umemoto, T., et al. 1993, in preparation
Ungerechts, H., et al. 1992, in IAU Symp. 150, The Astrochemistry of Cosmic Phenomena, ed. P. D. Singh (Dordrecht: Reidel), in press
Wilking, B. A., Lada, C. J., & Young, E. T. 1989, ApJ, 340, 823
Wouterloot, J. G. A., Walmsley, C. M., & Henkel, C. 1988, A&A, 203, 367
Zhou, S., Wu, Y., Evans, N. J., II, Fuller, G. A., & Myers, P. C. 1989, ApJ, 346, 168
Zinnecker, H. 1990, in Physical Processes in Fragmentation and Star Formation, ed. R. Capuzzo-Dolcetta, C. Chiosi, & A. Di Fazio (Dordrecht: Kluwer), 201
Ziurys, L. M., Wilson, T. L., & Mauersberger, R. 1990, ApJ, 356, L25